

REVIEWS



Engineering high-coherence superconducting qubits

Irfan Siddiqi^{1,2}

Abstract | Advances in materials science and engineering have played a central role in the development of classical computers and will undoubtedly be critical in propelling the maturation of quantum information technologies. In approaches to quantum computation based on superconducting circuits, as one goes from bulk materials to functional devices, amorphous films and non-equilibrium excitations — electronic and phononic — are introduced, leading to dissipation and fluctuations that limit the computational power of state-of-the-art qubits and processors. In this Review, the major sources of decoherence in superconducting qubits are identified through an exploration of seminal qubit and resonator experiments. The proposed microscopic mechanisms associated with these imperfections are summarized, and directions for future research are discussed. The trade-offs between simple qubit primitives based on a single Josephson tunnel junction and more complex designs that use additional circuit elements, or new junction modalities, to reduce sensitivity to local noise sources are discussed, particularly in the context of materials optimization strategies for each architecture.

Classical information processing technologies have deep roots in many decades of advanced materials engineering. The purification and doping of silicon and compound semiconductors, the robust and defect-free patterning of submicrometre metallic wiring, and the removal of impurities from surfaces and interfaces have been integral in producing transistor counts above 10 billion in modern processors, each with dimensions approaching a regime where quantum mechanical effects are manifest. Miniaturization introduces new microscopic quantum effects in a transistor on top of those related to the motion of electrons in solids, and mastering them will be important for further miniaturization of field-effect transistors. On a completely different level, macroscopic quantum effects in solid-state devices, in particular the fact that currents and voltages are quantum variables, can be used to push new developments in information physics towards the realization of quantum computers. Achieving a quantum computational advantage will require a full-scale redesign of the materials and wiring layers in a processor, targeting the generation, preservation and control of many-body entanglement^{1,2}. Advances in the synthesis, patterning and efficient characterization of a broad range of materials systems with long-lived, programmable coherence are thus critical to the implementation of quantum information technologies, particularly given the fact that the processor architecture representing the most robust and practical route to building a universal quantum computer, and the recipe to fabricate it, have yet to be identified.

In a quantum processor, the basic postulates for manipulating information are fundamentally different from those valid for its classical cousin, and they strongly influence the choice of materials and nanofabrication methods. In conventional logic devices, it is advantageous to pack as many bits per unit volume as possible while minimizing any coupling between them. Crucially, dissipation is a resource that can be used to suppress noise and crosstalk, albeit at the expense of energy efficiency. In a quantum architecture, the situation is more complex, as specific combinations of multiple qubits must be jointly addressed on demand to create a level of correlation that exceeds classical statistical bounds³, while also eliminating crosstalk between idle qubits and any excess dissipative elements that result in unintended loss of information. Such entangled states cannot be described by concatenating independent descriptions of each constituent qubit, and form the backbone of an accessible computational space that maximally grows as 2^N for N qubits. Notably, 300 or so fully entangled, perfect qubits would require more numbers than there are particles in the known Universe for a complete description: algorithms that take advantage of this exceptionally rich structure of encoded information promise unprecedented computing power. The caveat, however, is that quantum entanglement is extremely fragile, being readily transferred to other physical systems that we cannot either control or measure, resulting in decoherence⁴, which limits the lifetime of a complex quantum state and correspondingly the number of gate

¹Department of Physics,
University of California,
Berkeley, CA, USA.

²Computational Research and
Materials Sciences Divisions,
Lawrence Berkeley National
Laboratory, Berkeley,
CA, USA.

e-mail: irfan@berkeley.edu
[https://doi.org/10.1038/
 s41578-021-00370-4](https://doi.org/10.1038/s41578-021-00370-4)

operations that can be faithfully executed in a quantum algorithm. At the same time, quantum processors cannot be completely isolated from the environment, as information needs to be shuttled in and out of the system to perform and record a computation. The fundamental design challenge is thus to maintain coherence without compromising high-fidelity quantum logic operations and qubit readout. It is important to note that quantum systems not only require protection from the garbling of information between the two states of a qubit, but also the suppression of information loss out of this simple two-state computational space — a challenging problem to rectify using current quantum error correction codes⁵.

Nonetheless, progress towards sustaining quantum effects in electrical circuits of growing complexity has

been remarkable, with superconducting quantum processors not only rapidly growing in qubit count and functionality⁶, but also demonstrating a five-orders-of-magnitude improvement in coherence times⁷ in few-qubit circuits compared with the first demonstration of coherent time-domain measurements in 1999 (REF.⁸) (FIG. 1a). Contemporary superconducting qubits combine one or a few Al/AlO_x/Al Josephson junctions (JJs), which function as a nonlinear inductance⁹, with other reactive elements — comprising thin-film Al, Nb, NbN, NbTiN, Ta or TiN, for example — to form a circuit where the potential energy surface has at least two bound states. The minimalist realization of such an anharmonic oscillator is a single Josephson tunnel junction, formed by two planar superconducting electrodes separated by an insulating layer. The geometric self-capacitance shunts the kinetic inductance associated with Cooper pairs tunnelling across the barrier to yield a resonance frequency typically in the microwave frequency range, and individual quantum levels can be readily detected using microwave spectroscopy^{10,11}. Coupling the JJ circuit to a microwave resonator for control and readout robustly yields long-lived charge-based and flux-based qubits in which the lowest two energy levels form the ‘0’ and ‘1’ states of a physical qubit^{12,13}. In these circuits, the junction provides the anharmonicity needed to selectively address the 0–1 transition. JJs can be constructed by sandwiching two superconducting reservoirs around any structure that allows the condensate wavefunction to deviate from its surrounding bulk value, but the tunnel-junction geometry with an insulating barrier has thus far been the most widely used¹⁴ in electronic circuits given the attractive features of a robust sinusoidal dependence of the supercurrent on the junction phase difference¹⁵ and the absence of electronic states below the superconducting energy gap. To tune the qubit parameters and drive quantum state transitions, JJs can be readily integrated into superconducting loops, or can be contacted with isolated submicrometre superconducting islands, enabling control via an external magnetic or electric field, respectively^{16–19}.

The design space for superconducting qubits is thus very rich, with many possible circuit variants^{20,21}. The basic oscillatory circuit described above can be integrated with additional reactive elements to modify its characteristic impedance and associated coupling to the environment¹⁹. Furthermore, the area of the JJs, as well as the size and dimensionality of the passive microwave frequency elements embedding them, can be adjusted to trade between free-space radiation loss and surface loss^{22–24}. Finally, with the additional freedom to use multiple junctions per qubit, JJs can be arranged to engineer specific symmetries and non-trivial topologies into the circuit to achieve varying degrees of noise protection²⁵. Generally speaking, structures that use fewer junctions and leverage circuit designs that can operate over a broad range of tunnel resistances potentially offer an easier route to robust manufacturing, but at the cost of being susceptible to a wider range of decoherence mechanisms. Different qubit types thus have varying degrees of coupling to environmental noise, and each specific circuit architecture presents unique materials

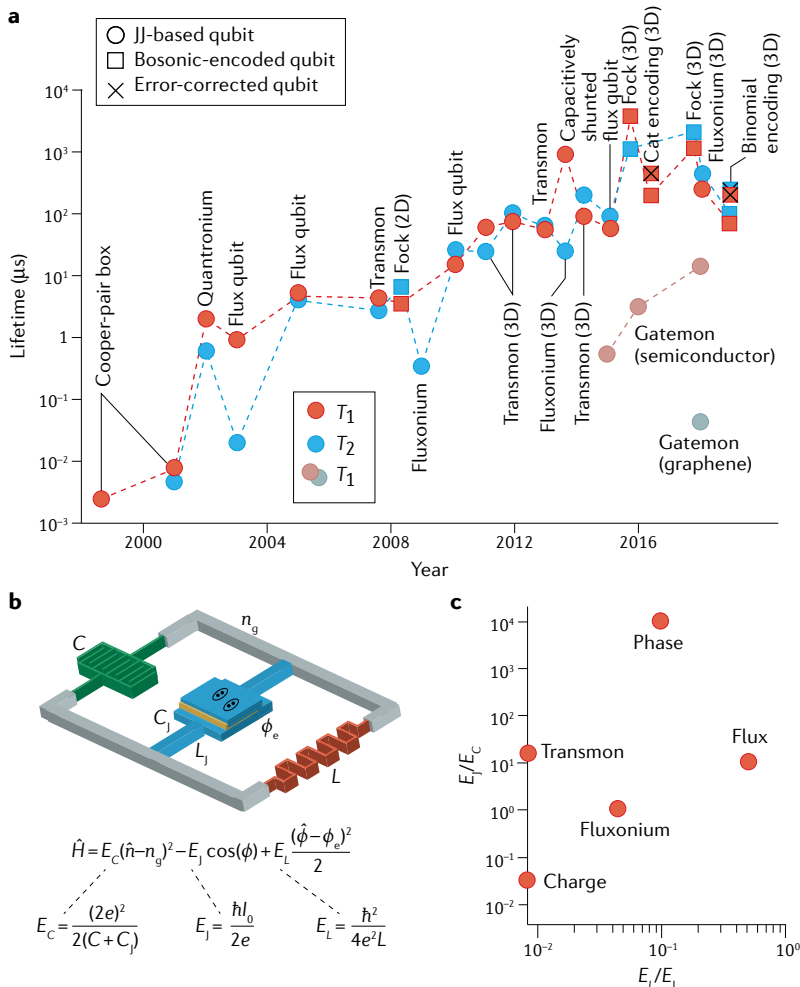


Fig. 1 | Superconducting qubits. **a** | Coherence data (T_1, T_2) reported over the past two decades for Josephson junction (JJ) circuit qubits, including architectures encoding information in microwave cavity photons and devices using error mitigation. T_1 is the characteristic time for energy relaxation, and T_2 quantifies decoherence due to both energy relaxation and dephasing. **b** | Equivalent circuit and associated Hamiltonian for common superconducting qubits consisting of a Josephson junction (blue) described by a geometric capacitance and an inductance associated with Cooper-pair tunnelling, a linear shunt capacitor (green) and a shunt inductance (red). **c** | Categorization of qubits based on their charging, Josephson and inductive energies (E_C, E_J and E_L , respectively). ϕ , phase difference across the junction; ϕ_e , offset phase; C , capacitance; C_j , junction capacitance; I_{J_c} , junction critical current; L , inductance; L_j , junction inductance; \hat{n} , island charge; n_g , offset charge bias. Panel **a** is adapted with permission from REF.¹⁸, Annual Reviews.

optimization challenges and trade-offs. Conversely, coherence data from these devices offer complementary information about the underlying sources of decoherence present in superconducting circuits.

Suppressing decoherence — information loss that results from energy relaxation and a garbling of the phase — involves a synchronous optimization of both materials quality and electromagnetic design¹⁹. In electrical circuits, resistive metals dissipate locally stored energy into a bath that cannot be accessed and ultimately thermalizes. Although swapping superconductors for normal conductors eliminates the bulk of this loss, any other structures, such as circuit elements used for readout and control, that comprise a real-valued shunting admittance must also be distanced from quantum coherent elements²⁶. Furthermore, ideal qubit circuits would be coupled to highly stable microwave electronics, use phase-stable coaxial cables and waveguides, and be designed to have vanishing coupling to both non-radiative and radiative spurious modes of the chip and its cryopackage. In practice, after careful quantum engineering to minimize imperfections attributable to circuit design, significant decoherence still results from materials defects in thin metallic films, lossy and noisy dielectrics, and remnant layers of unwanted thin-film amorphous materials — naturally forming on unpreserved surfaces or inadvertently grown during nanofabrication — that contribute to the degradation of quantum information^{27,28}. Moreover, although operation at millikelvin temperatures should freeze out electronic and vibrational degrees of freedom, a substantial population of non-equilibrium excitations²⁹ is observed, constituting a significant source of decoherence^{11,30}.

In this Review, the main sources of materials-related decoherence observed in superconducting qubits of varying degrees of circuit complexity are introduced, along with our current understanding of the microscopic physics underlying these noise sources. We start by describing the circuits that form the basis of conventional Josephson tunnel-junction qubits and listing their suspected sources of imperfection. We then examine the decoherence mechanisms in such devices, providing a high-level theoretical description followed by a synopsis of select experimental results that splice coherence data from different superconducting qubit architectures and microwave frequency resonators, before summarizing best practices and raising key outstanding materials science questions for each decoherence mechanism. We then introduce noise-protected structures that incorporate symmetry and complex topology, and finally discuss emerging qubit architectures that use non-conventional superconducting junctions. We conclude by positing possible directions for both near-term materials optimization and broad topics for future research.

Conventional Josephson tunnel-junction qubits

We start by detailing the basic design and operation of superconducting qubits containing one or more tunnel junctions embedded within reactive circuit elements³¹. Many of these circuits have several quantum energy levels in a nonlinear potential and can, in general, function as qudits with three^{32,33} or more logical states, but we

will focus on a simple qubit description to frame our discussion of materials optimization. At low excitation power in the zero-voltage or ‘superconducting’ state, the tunnel junction is characterized by an effective inductance $L_J = \hbar/(2eI_0 \cos(\phi))$, where I_0 is the material- and geometry-dependent junction critical current and ϕ is the phase difference across the junction. The supercurrent through the junction is given by the d.c. Josephson relation, $I(\phi) = I_0 \sin(\phi)$, and its magnitude increases nonlinearly with ϕ , with a corresponding increase of the inductance L_J . We can define the characteristic energy associated with each Cooper pair tunnelling event as $E_J = (\hbar/2e)I_0$. The geometric capacitance of the junction itself is denoted by C_J . Typical Al/AlO_x/Al junctions with an amorphous ~1-nm-thick tunnel barrier have been the workhorse of the community thus far. Even though Al has a considerable lattice mismatch with Al₂O₃, the sandwich has proven remarkably robust in terms of reproducible electrical characteristics, with a variability of 5–25%³⁴ across arrays of nominally identical junctions. Coherence times in modern submicrometre JJ qubit designs are typically limited by dielectric defects, radiative loss or quasiparticles. Moreover, the presence of polycrystalline electrodes and a non-stoichiometric, metastable barrier results in the variable ageing of tunnel resistances post-fabrication at room temperature, a high sensitivity to precise conditions for deposition and so on, and the often-observed presence of strongly coupled two-level-system defects. These shortcomings need to be addressed in the near term as qubit counts increase, with the goal of achieving defect-free devices with less than 1% dispersion of parameter values.

Using an additional capacitor C connected across the junction electrodes, it is possible to reduce the plasma frequency of the junction, originally set by $1/\sqrt{L_J C_J}$, to the 1–10 GHz range to avoid the complexity of controlling microwave circuit impedances at frequencies much higher than 10 GHz. The capacitor paddles form isolated superconducting islands, and the total electrostatic charging energy, expressed in terms of the Cooper-pair charge $2e$, is $E_C = (2e)^2/2(C + C_J)$. In the presence of an applied voltage, an offset charge bias n_g can be applied to these islands. The junction may also be inserted into a loop with a shunt inductance L and an associated energy $E_L = \hbar^2/(4e^2 L)$. Threading the loop with an external magnetic field applies an offset phase ϕ_e to the junction. These three circuit elements — the JJ, the capacitor and the inductor — define an archetypal equivalent circuit for common superconducting qubits²⁰ (FIG. 1b). The Hamiltonian for this circuit can be written in terms of operators characterizing the charge of the island \hat{n} and the phase difference across the junction $\hat{\phi}$. The kinetic energy term is associated with the Coulomb energy, with the total capacitance acting as an effective mass and the inductive elements — the junction and the linear shunt inductor — defining the potential energy.

Common qubits

In the Hamiltonian above, the dynamics characteristic of a qubit circuit can be described by the motion of a fictitious particle in a potential $U(\phi) = -E_J \cos(\phi) + E_L(\phi - \phi_e)^2/2$. The fauna of superconducting qubits that inhabit this

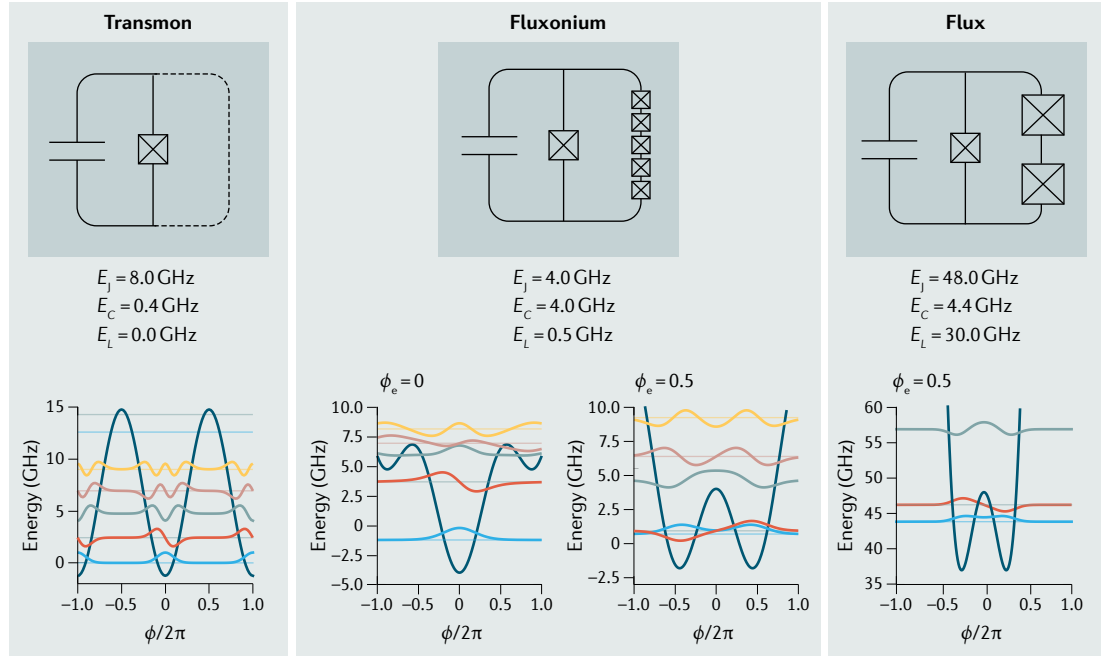


Fig. 2 | Qubit types. Equivalent circuits and their associated potential energy surfaces (dark blue) with the low-lying wavefunctions (other colours) for a typical transmon, fluxonium and flux qubit. The parameter values used in the calculations are indicated and reflect values found in the literature. ϕ , phase difference across the junction; ϕ_e , offset phase; E_C , charging energy; E_J , Josephson energy; E_L , inductive energy.

potential landscape can be categorized by the ratios E_J/E_C and E_L/E_J (FIG. 1c). The phase qubit^{35,36} is essentially a large-area ($\gtrsim \mu\text{m}^2$) junction with a pF overlap shunt capacitor incorporated into an inductive loop. To tune the energy levels of the qubit, a current bias is applied through a superconducting flux transformer. Phase qubits have a large E_J/E_C ratio, typically bigger than 10^4 . In the opposite limit, charge qubits³ have a E_J/E_C ratio much smaller than 1. The transmon design^{12,37} is a ‘charge-insensitive’ charge qubit that operates with $E_J/E_C \sim 10–100$, resulting in a weakly nonlinear oscillator with an exponential suppression of the sensitivity of the qubit frequency to slow charge fluctuations and only a weak power-law reduction of the oscillator anharmonicity. Typical devices only have a few hundred MHz separation in the transition frequencies between adjacent levels, and fast gate pulses with a wide spectral content can result in leakage to the higher levels of the transmon. The transmon has no inductive shunt ($E_L=0$) and the qubit states are the lowest levels of a purely cosine potential. Inductively shunting the JJ with two larger junctions results in a flux qubit³⁸. Shunting with a large array of junctions to realize a much larger inductance is the basis of the fluxonium^{39–41} design. Both of these inductively shunted qubits can also be capacitively shunted^{13,42} to further suppress charge fluctuations. For the flux and fluxonium qubits, $E_L \sim E_J$ and the potential energy function is a sinusoidally modulated parabola that can be biased with an external magnetic flux to tune the shape of the bottom of the potential to have either a single or a double well. Simplified equivalent circuits for the transmon, fluxonium and flux qubits along with their associated potential energy wells and calculated wavefunctions are shown in FIG. 2 for common circuit parameters.

In terms of noise sensitivity, phase qubits use large-area capacitors and junctions and are a good platform to study decoherence from amorphous dielectric layers; charge qubits can serve as quasiparticle detectors; and flux-tunable qubits are exquisite magnetometers and sensitive probes of phase-dependent phenomena.

We now consider circuitry for driving transitions between states of a qubit, entangling disparate qubits, and reading out quantum states. A transmission line terminated in an open circuit or short circuit readily delivers a high-frequency oscillating voltage or current, respectively, for quantum control. Resonators (either planar and directly integrated on the qubit chip^{43,44} or realized by a 3D cavity³⁷) can interact with a qubit via the Jaynes–Cummings Hamiltonian⁴⁵, which allows for information to be exchanged between the qubit and the electromagnetic field of the resonator. Thin-film devices consisting of Al or Nb/Nb-alloys have a quality (Q) factor — the ratio of energy initially stored in the resonator to the energy lost in one cycle — that are in the range 1 million to 10 million for a single quantum excitation; 3D cavities have several orders-of-magnitude lower loss. This level of coherence is sufficient to faithfully observe and swap quantum information. If the frequency of the qubit and resonator are commensurate, it is possible to obtain a single, hybridized, polariton-like system. When the qubit and cavity are sufficiently detuned, the circuit is in the ‘dispersive limit’, where the frequency of the resonator can be viewed as being shifted in a digital fashion depending on the state of the qubit or vice versa. This duality allows quantum information to be encoded in either the states of the JJ circuit or in the photons of the cavity⁴⁶. For the latter case, we note that microwave photons in high-quality cavities can be extremely long-lived

and are a powerful resource for photonic qubits, in which the nonlinearity of the junction enables state-selective quantum control. Furthermore, there are also a number of architectures that lie between purely 2D and 3D designs: multilayer devices based on through-Si vias, flip-chip modules and micromachined resonators^{47–49}. From a technological perspective, advances in fields targeting compact multi-qubit devices will play a key role in bringing scalable quantum information processing hardware to market, providing additional pathways, for example, to eliminate or distance noisy dielectric interconnects. Many of the basic design principles, materials imperfections identified and mitigation pathways suggested in the context of matter-based qubits in this Review are also relevant for these cavity-focused architectures, which also consist of thin superconducting films and Josephson junctions.

Sources of imperfection

In an ideal qubit circuit, all elements would be in thermal equilibrium with a cryogenic bath and have minimal losses to any radiative modes. The insulators would possess a large bandgap for electronic excitations, and the metallic superconducting structures would have a uniform energy gap equal to the value observed in bulk. In practice, however, qubits have a number of materials imperfections that contribute to decoherence (FIG. 3). Insulating materials (for example amorphous silicon, a-Si (REF.⁵⁰), silicon oxides, SiO_x (REF.⁵¹), and nitrides, Si-N_x (REF.⁵²), aluminium oxide, AlO_x (REF.⁵³) and niobium pentoxide, NbO_x (REF.⁵¹)) used for electrical isolation in wiring layers and for capacitor dielectrics are typically amorphous, and generally exhibit noise that is believed to be caused by two-level-system (TLS) defects^{54,55}. Unwanted thin amorphous layers are generated not only upon atmospheric exposure, but also during various fabrication steps, including plasma-assisted deposition and etching. Moreover, the junction tunnel barrier itself is almost exclusively a ~1-nm layer of amorphous AlO_x. Finally, metal surfaces including the junction electrodes and passive microwave components generally comprise polycrystalline films that form native amorphous oxides (FIG. 3b). These surface layers are suspected also to host paramagnetic defects that contribute to low-frequency 1/f flux noise (FIG. 3c). The type and intensity of decoherence resulting from these different amorphous layers depend on whether the qubit couples to a single defect or an ensemble, on the defect density and on the device geometry, particularly through the ‘participation ratio’, which quantifies the fraction of the electromagnetic field that couples to defects. In addition, the metallic structures in a superconducting circuit are not lossless. In a bulk type-I superconductor, magnetic fields are screened by the Meissner effect. Thin-film structures, however, can trap vortices in the presence of a non-zero magnetic field. Additionally, although the superconducting energy gap protects against dissipation at low frequencies, Cooper pairs may be readily broken when exposed to infrared⁵⁶ or ionizing radiation⁵⁷ leaking into the cryostat, generating non-equilibrium quasiparticles and phonons (FIG. 3d).

These common decoherence mechanisms are summarized in FIG. 3b–e. We can visualize their action on

a qubit by representing the quantum state of a single qubit on a unit (Bloch) sphere where an arbitrary superposition is represented by a point on the surface, and the poles along the z-axis represent the two eigenstates |0⟩ and |1⟩ (FIG. 3e), much like a spin subject to a Zeeman magnetic field applied vertically. Defects can cause energy relaxation processes, which can be viewed as resulting from a noise source in the x-y plane that causes a rotation taking |1⟩ to |0⟩. This process is characterized by an average time and rate T_1 and Γ_1 , respectively. A slowly varying noise environment contributes to dephasing, characterized by an average time and rate T_ϕ and Γ_ϕ , respectively. Dephasing can be viewed as resulting from noise in the z-direction that rotates a vector in the x-y plane along the equator. The combination of these two processes contributes to the decoherence time T_2 , which can be expressed as $T_2^{-1} = (2T_1)^{-1} + T_\phi^{-1}$ when the noise bath embedding the qubit circuit can be approximated as Markovian⁵⁸.

Sources of decoherence

Two-level-system defects

The tunnel barrier in a conventional Al/AlO_x/Al JJ, oxides formed on the metallic surfaces of Al and Nb, and thin-film dielectrics used to form capacitors and insulating layers are believed to be laden with TLS defects^{59,60} that exhibit glass-like behaviour. Although not all amorphous films need be a priori deleterious, and crystalline materials can harbour dislocations, vacancies or interstitial impurities, imperfections formed in the absence of long-range crystalline order and in the presence of two configurations with similar energies are believed to give rise to local defect sites throughout the thin films. The basic phenomenological description for TLS defects is based on a standard tunnelling model⁶¹ with an asymmetric double-well potential^{62,63} whose lowest levels represent two possible atomic or electronic configurations. A review by Clemens Müller and colleagues²⁸ highlights many aspects of TLS physics in the context of quantum circuits. An ensemble of TLS defects is believed to be responsible for a number of different decoherence mechanisms, including energy relaxation over a broad frequency band when the TLS energy splitting is commensurate with the operating frequency of a quantum circuit, dephasing due to low-frequency fluctuations^{64,65} and the slow drift of coherence times⁶⁶. Classic experiments using superconducting qubits and resonators that directly support the TLS model sketched above and implicate these defects in various decoherence processes are highlighted in this section. These experiments exhibit the quintessential features of the TLS model: the observation of avoided crossings in qubit spectroscopy, strain-tuning of TLS defects and the saturation of TLS loss with applied power.

Although the precise microscopic details of the TLS defects themselves are still only conjectured, a phenomenological treatment is a starting point to model a wide range of observed phenomena²⁸. We start by analysing the canonical potential energy surface for a TLS, where the TLS configurations are represented by two local minima, denoted |L⟩ and |R⟩ for left and right, separated by a distance d and an energy

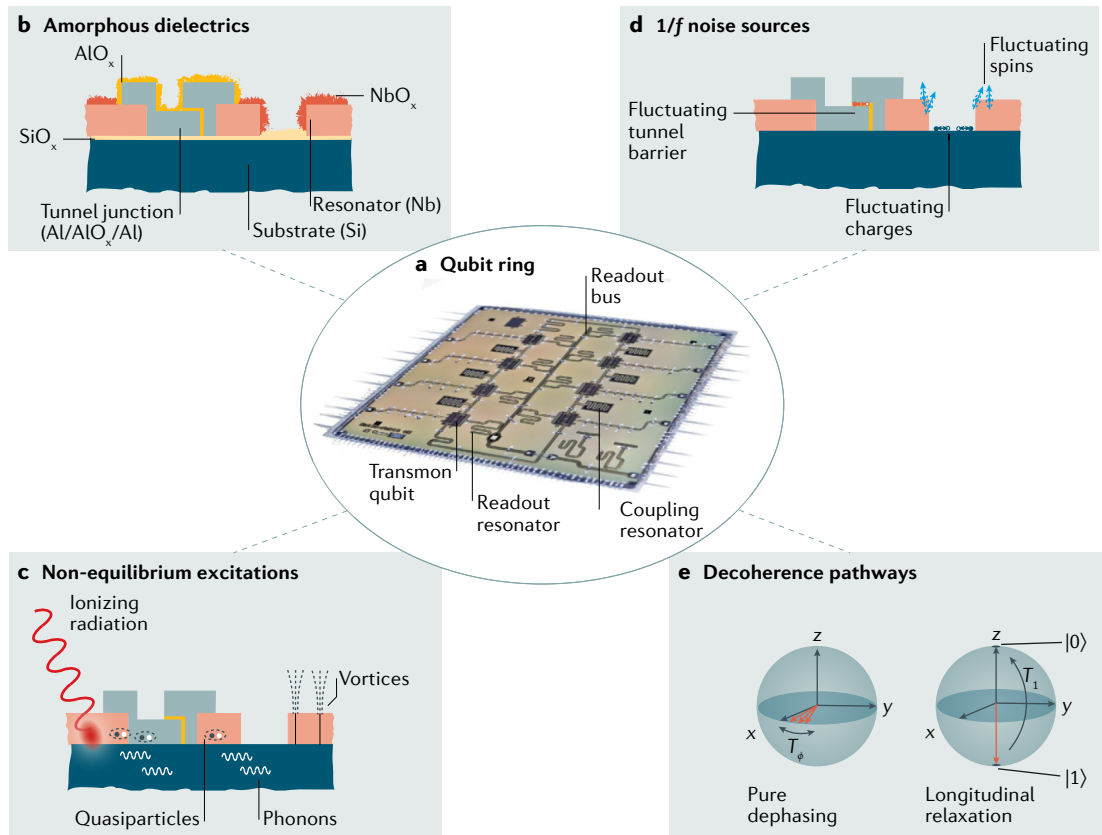


Fig. 3 | Sources of decoherence. **a** | Optical image of a qubit ring consisting of eight transmons with Al/AlO_x/Al Josephson junctions (JJs) and an Nb microwave embedding circuit. Each qubit is coupled to its neighbour via a resonator. An additional resonator allows for quantum state readout and multiplexing to a common bus. **b** | Decoherence can result from surface and interfacial defect layers; the schematic identifies specific amorphous layers. **c** | Non-equilibrium excitations of the superconducting films and substrate can arise from ionizing radiation and remnant magnetic fields. In particular, these noise sources generate quasiparticles, hot phonons and vortices. **d** | Microscopic charge and spin defects are believed to give rise to 1/f fluctuations that bias the qubit circuit with a varying electric or magnetic field, or cause jitter in the JJ inductance if defects are present in the tunnel barrier. **e** | Fluctuations in the environment can drive qubit transitions if the noise is orthogonal to the qubit axis (longitudinal relaxation) or pure dephasing if it is aligned with the qubit axis. The characteristic time constants for these processes, following NMR nomenclature, are T_1 and T_ϕ , respectively. Image in the central panel courtesy of J. M. Kreikebaum, Berkeley.

barrier V (FIG. 4a). These minima differ in energy by ϵ , reflecting a different electronic environment in each configuration, and the right and left wells are connected via a tunnel coupling Δ . The energy difference between the two lowest hybridized levels is given by $E = \sqrt{\epsilon^2 + \Delta^2}$, and the canonical TLS Hamiltonian can be expressed in terms of Pauli operators in the position basis as $\epsilon\sigma_z/2 + \Delta\sigma_x/2$. Here $\sigma_z = |\mathcal{R}\rangle\langle\mathcal{R}| - |\mathcal{L}\rangle\langle\mathcal{L}|$, $\sigma_x = |\mathcal{R}\rangle\langle\mathcal{L}| + |\mathcal{L}\rangle\langle\mathcal{R}|$, and the two lowest eigenstates are given by $|\Psi_\pm\rangle = \cos(\theta/2)|\mathcal{L}\rangle \pm \sin(\theta/2)|\mathcal{R}\rangle$, where $\theta = \tan^{-1}(\Delta/\epsilon)$. In the limit $|\epsilon| \gg \Delta$, the model simplifies to two localized states, one in each of the two wells, whereas when $|\epsilon| \approx 0$ we have a superposition of the right and left states. It is possible to approximate the tunnel coupling using semiclassical methods, resulting in $\Delta \propto e^{-kd}$ with $k = \sqrt{2mV/\hbar^2}$ and m the effective mass of the TLS. We assume that when operating at millikelvin temperatures, activation over the TLS potential barrier is negligible and quantum tunnelling is dominant.

We now extend this model to the case when many such TLS defects are distributed in an amorphous film.

Because these imperfections are not like defect states in a crystalline material, which may be identical from site to site, we assume that the local environment for each TLS is random, and thus the distributions of ϵ and V , and therefore the decay length k , are broad and uniform. The probability density of a certain trap energy asymmetry and decay length is $P(\epsilon, k)dkd\epsilon = P_0 dk d\epsilon = (P_0/\Delta)(E/\sqrt{E^2 - \Delta^2})d\Delta dE$, where P_0 is a constant. This distribution of energy biases and well heights gives rise to a constant density of defect states when integrating over possible values of Δ , which are presumed to scale from a very low value, corresponding to the slowest dynamics in the system, up to the energy E . Additionally, the log-uniform distribution of $P(E, \Delta) \propto 1/\Delta$ is compatible with a spectral density of fluctuations that can produce 1/f noise at low frequencies and ohmic dissipation at high frequencies $\hbar\omega \gg k_B T$ (REF.⁶⁷). Thus, we expect that TLS defects may reduce both T_1 and T_ϕ in the presence of both transverse and longitudinal coupling to a qubit (FIG. 4b). It is important to note that this simple model is just a starting point, and a variety

of qubit and resonator experiments exhibit important deviations not compatible with this basic description alone. Some of these results are discussed below, including drifts in coherence times that imply, along with other experimental signatures, that TLS–TLS interactions are significant, and the presence of a frequency dependence in the simple defect density derived above.

Qubit measurements. We start by presenting qubit measurements that strongly indicate the presence of TLS defects. Consider first the case where a TLS is coupled to a qubit with strength g , such that g is larger than the decoherence rate of both the TLS and the qubit. In this regime, the TLS essentially acts as a random qubit that can swap information with the quantum circuit when the two are in resonance. Phase qubits consist of a large-area JJ and an overlap shunt capacitor, both with lateral dimensions exceeding a micrometre, and therefore have large areas of amorphous thin films with many TLS defects. Smaller junctions exhibit proportionately fewer defects. Moreover, it has been posited that submicron junctions have even a lower defect density than one would predict by simply scaling junction area on account of comparatively less strain. More work is needed to directly verify this conjecture. When such defects are exposed to an intense electric field when the circuit is energized, they give rise to a classic signature of TLS physics: avoided crossings directly observed in qubit spectroscopy, indicating strong electromagnetic coupling to many distinct TLS defects^{68,69} (FIG. 5a). Signatures of this strong coupling can also be observed in the time domain, where beating behaviour is seen when driving coherent Rabi oscillations or performing a Ramsey fringe sequence⁷⁰.

The standard tunnelling model can be used to derive an equation for the number of observed splittings N in

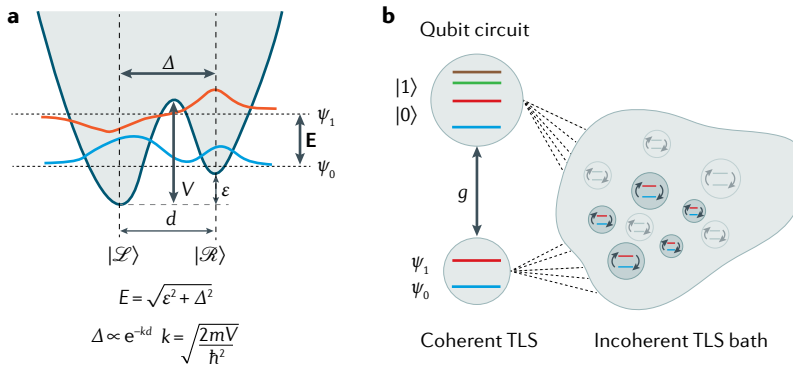


Fig. 4 | TLS defects. **a** Two-level-system (TLS) dynamics, in a simplified picture, can be modelled as tunnelling in a double-well potential. The distribution of defects as a function of the tunnel splitting Δ and energy E is approximated as a log-uniform distribution in Δ , assuming that there exists a broad, uniform distribution of barrier heights V and asymmetries ε . **b** Coherent TLSs have an energy splitting commensurate with that of the qubit, and the two exchange information at rate g , resulting in energy relaxation. Incoherent TLSs have an energy spacing much smaller than the thermal energy, and, when coupled to a qubit, present a bath with low-frequency fluctuations that results in qubit dephasing. Coherent TLS can also couple to such a bath, and TLS–TLS interactions are believed to result in a fluctuating noise intensity seen by the qubit (spectral diffusion), potentially causing drifts of qubit coherence times. It is important to note that TLS–TLS interactions and deviations from a frequency-independent distribution of defects observed in some experiments require a more elaborate model than the simple, isolated TLS description described above.

a phase qubit: $d^2N/dEdg = \sigma A \sqrt{g^2 - g_{\max}^2}/2g$, where σ is the areal density of defects for a particular lossy dielectric, A is the junction area and g_{\max} is the largest observed splitting⁶⁹. This formula produces results in good agreement with the data shown in FIG. 5a, further supporting the basic premise of the TLS hypothesis. For large Al/AlO_x/Al junctions, reported values of the areal density are approximately $\sigma \approx 1/(GHz \mu m^2)$ ^{69–72}. Notably, the splitting density is much smaller for the submicrometre junctions used in transmon and xmon⁷³ qubits. Moreover, qubits that incorporate submicrometre junctions, planar capacitors, and minimalist wiring layers and dielectrics only occasionally exhibit strongly coupled, individually addressable TLS defects, although as the qubit count increases in a processor, observing such defects in every chip becomes fairly probable. The presence of TLS defects with weaker coupling strengths that are not resolved in spectroscopy can be indirectly inferred through reductions of the coherence time at specific frequencies. Finally, thermal cycling of qubit devices shifts the inferred TLS resonance frequencies, supporting the idea that these defects are randomly formed in amorphous layers.

Time-domain measurements indicate a strong correlation between TLS density and coherence times, with improvements observed in both energy relaxation and dephasing times when high-quality dielectric films are incorporated into qubit circuits⁶⁶. For dephasing processes, one envisages the qubit coupling to a bath of TLS defects that are themselves rapidly flipping between their states on account of interactions with a noisy environment (FIG. 4b). Coupling to phonons, other TLSs, and quasiparticles may be the cause of this TLS decoherence. These rapid oscillations collectively present themselves to the qubit as a low-frequency, potentially 1/f-type, noise source⁷⁴. Additional qubit decoherence processes may arise if TLS defects interact with each other. We can envisage a spectral diffusion process where a TLS with long-lived coherence, sufficient to swap information with a qubit, itself couples to a rapidly fluctuating TLS bath, causing the resonant frequency of the qubit to fluctuate⁷⁵. In this scenario, a qubit coupled to the first TLS will experience a time-varying noise environment. This mechanism may account for the slow variation of T_1 and T_2 times seen in nearly all superconducting qubits^{76,77}.

The qubit experiments described above used electrical tuning of the qubit frequency to realize an effective TLS spectrometer. It is also possible to directly tune the energy splitting of a TLS using an applied strain field. Recent experiments have used this control mechanism by mechanically bending the qubit substrate to tune TLS frequencies⁷⁸. The ground-state energy of each of the two TLS states couples to strain and local phonons; the energy asymmetry ε is proportional to $\gamma \cdot S$, where S is the strain field and γ the direction-dependent coupling strength. Strain-field spectroscopy⁷⁹ clearly indicated the presence of a large quantity of TLS defects in a phase qubit (FIG. 5b). Additionally, critical direct evidence for TLS–TLS coupling is seen in both telegraph noise and avoided crossings⁸⁰. These measurements indicate coupling strengths γ in the 0.1–1.0 eV range, in line with previous studies of glassy materials.

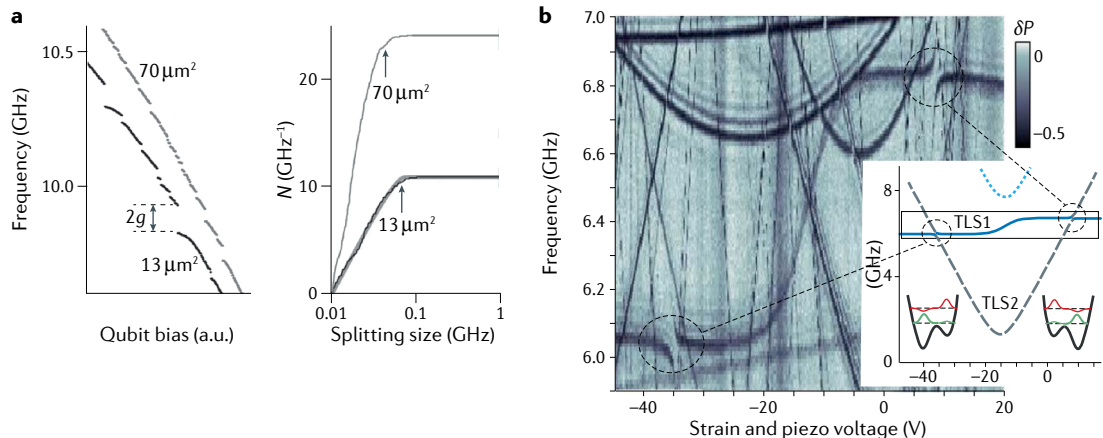


Fig. 5 | Experimental evidence for TLS defects. **a** | Avoided crossings in microwave spectroscopy point to the presence of strongly coupled two-level-system (TLS) defects. Here, a magnetic flux bias is applied to sweep the qubit resonance frequency in two samples with junction areas of 13 and $70\mu\text{m}^2$. Strong interactions with TLS defects result in avoided crossings with coupling strength g . N is the number of observed splittings. **b** | Adding a strain field via mechanical control reveals a rich spectrum of TLS defects, as inferred by a drop in the qubit population P when interacting with a TLS. Moreover, we see signatures of TLS–TLS interactions. Here, the bias directly tunes the TLS frequencies, and avoided crossings indicate strong interactions between different TLS defects. Panel **a** is reprinted with permission from REF⁶⁹, American Physical Society. Panel **b** is adapted from REF⁸⁰, CC BY 4.0.

Resonator measurements. Decoherence from TLS defects, particularly ensemble effects, is also observed in high- Q microwave resonators⁸¹. TLS defects induce energy loss in qubit-embedding circuits in the single quantum excitation regime⁸² and excess phase noise in microwave kinetic inductance detectors^{83,84}. Varying the geometry of coplanar waveguides and lumped-element circuits helps to pinpoint the relative contributions of amorphous layers on top of metal surfaces and at the metal/substrate interface, and permits an estimation of the microwave loss tangent δ of these lossy layers^{85–88}. The best a-Si and a-SiN films exhibit values approaching 10^{-5} , and other materials such as SiO_x typically hover around 10^{-3} – 10^{-4} . Recent measurements that combined materials characterization and coherence measurements revealed a direct correlation between the presence of surface oxides and diminished resonator Q (REFS^{89,90}). Similar to the qubit case, TLS–TLS coupling is believed to result in both frequency jitter and Q fluctuations of a resonator. Frequency noise results in a phase noise contribution that can limit the sensitivity of dispersive microwave detectors^{91,92}. Finally, we note a hallmark of TLS defects at low temperatures that is readily observed in resonators: a power-dependent loss⁵³. When TLS defects are flopping at a Rabi frequency faster than their decoherence rate, they effectively saturate and their impact on Q is minimal. Additionally, the dielectric loading of a TLS bath is higher when these defects are in the ground state, resulting in a power-dependent and temperature-dependent frequency shift. Notably, this frequency shift also has a contribution from defects that are not resonant with the quantum circuit, allowing for the study of TLS decoherence beyond the single quantum excitation regime.

Materials characterization. The further reduction of TLS defects remains a key task for improving coherence times. Although the standard tunnelling model of

TLS defects can account for a wide range of decoherence phenomena observed in superconducting circuits, understanding the nature of TLS–TLS interactions and precisely identifying the detailed microscopic mechanism underlying such defects has proven tremendously challenging. There are a number of candidates for TLS defects: hydrogenated Al vacancies, interstitial hydrogen defects, dangling OH bonds on the surface that act as rotors, electrons dressed by phononic interactions, electrons trapped in metal–insulator gap states, quasiparticles hopping between disorder-mediated Andreev states⁹³ and several others²⁸. Note that not all of these candidates are simply linked to lossy dielectrics. Modern materials characterization techniques can help link possible TLS candidates to their influence on qubit coherence. Combining electrical characterization with imaging techniques, including high-resolution transmission electron microscopy, with analytical tools for elemental analysis, X-ray photoemission spectroscopy and time-of-flight secondary ion mass spectroscopy, it is possible to identify the thickness, elemental composition and stoichiometry of amorphous thin-film layers, leading to further refinement and validation of theoretical TLS models. Initial results on qubits and resonators in which the mitigation of amorphous films has been targeted have already demonstrated T_1 times in excess of 300 μs (REF.⁹⁴) and Q factors in excess of 5×10^6 for planar resonator^{89,90} and 10^{10} for 3D cavities⁹⁵. Further improvements are anticipated.

Viewing these results in aggregate, we can summarize a few recommendations for high-coherence materials design. If possible, dielectric materials should be placed in areas where the electromagnetic energy density is lowest, minimizing decoherence due to defects. Next, recipes for patterning and cleaning processes such as reactive ion etching and plasma cleaning should be tailored to reduce the thickness of process oxides formed

on top of superconducting films. These oxides can be removed, either with wet or dry etches, to improve coherence times, even in the presence of partial regrowth in ambient conditions. Notably, not all oxides are equally lossy. For example, there may be significant differences between Nb and Ta in this respect, and characterizing the microwave properties of these oxide layers is important. One may posit that metals that oxidize to produce near-stoichiometric, stable oxides are preferable to ones that have many metastable and/or semimetallic compounds. Finally, in circuits in which dielectric materials are needed, it has thus far been best to avoid using oxides of Si as insulating layers.

Quasiparticles

Theory predicts a vanishingly small equilibrium density of unpaired quasiparticle excitations at temperatures well below the superconducting critical temperature in a bulk superconductor with an isotropic energy gap, but this is manifestly not the case in thin-film quantum circuits. Assuming an equilibrium thermal distribution, the number density of quasiparticles is predicted to be $n_{qp} = 2N_0\sqrt{2\pi k_B T \Delta_0} \exp(-\Delta_0/k_B T)$, where N_0 is the single-particle density of states at the Fermi level and Δ_0 is the superconducting energy gap. For an Al or Nb film, this would correspond to an insignificant number of quasiparticles at 10 mK. However, a large body of experiments indicates that as the temperature of a quantum circuit is lowered, the quasiparticle density saturates at values of $n_{qp} \approx 10 - 100 \mu\text{m}^{-3}$ (REF.⁹⁶). Such an excess population of nonequilibrium quasiparticles can be attributed to several sources, including Cooper-pair breaking due to infrared radiation that leaks into the cryopackage housing the circuit and ionizing radiation such as muons and gamma rays. When electromagnetic radiation has an energy that is much higher than the superconducting gap, a cascade of scattering processes is believed to occur^{29,57,97}, starting with the excitation of high-energy phonons and quasiparticles that eventually scatter to the gap edge, thereby presenting a qubit with a complex time-dependent noise environment.

Qubit measurements. In qubit circuits, there are several fundamental effects that arise from the presence of a population of non-equilibrium quasiparticles and their number fluctuations. A detailed review of quasiparticle effects in superconducting qubits in various circuit topologies has recently been published by Leonid Glazman and Gianluigi Catelani³⁰. A simple circuit model for a JJ treats this element as a generalized complex admittance that is frequency-dependent and phase-dependent (FIG. 6a). There are four terms that describe the dispersive and dissipative effects of both Cooper pairs and quasiparticles. At zero-phase, this expression is equivalent to a Mattis-Bardeen⁹⁸, two-fluid model description of the complex a.c. conductivity of a superconductor⁹⁹. At the qubit frequency, quasiparticle excitations present a source of dissipation that enhances energy relaxation and thus reduces T_1 (REFS^{100,101}). For a phase qubit¹⁰², the associated energy relaxation rate is given by $1/T_1 = (1 + \cos(\phi))(\sqrt{2}eI_0/\pi)(\Delta_0/E_{01}^{3/2})(n_{qp}/n_{cp})$, where E_{01} is the energy of the qubit 0–1 transition and

the last term is the ratio of the quasiparticle density to the Cooper-pair density. The imaginary part of the admittance leads to a frequency shift of the qubit. In a classic phase qubit experiment¹⁰², quasiparticles were injected via a tunnel junction, and the relaxation rate and frequency shift were shown to be in good agreement with the expression for the junction admittance presented above (FIG. 6b). In particular, the onset of additional decoherence is observed when the bias current is intense enough to break pairs, strongly indicating that quasiparticles are indeed the source of the observed decoherence. Similar relations for energy relaxation and dephasing effects can be calculated for other qubits, including the transmon^{103,104}. The fluxonium qubit offers a very powerful circuit to explore the different components of the complex junction admittance, in particular the so-called Josephson cosine term, which describes a phase-dependent dissipation attributed to the interference of Cooper pairs and quasiparticles. If a flux bias can be applied¹⁰⁵, the contribution of quasiparticle dissipation is suppressed and a great enhancement of T_1 is observed at a bias of 1/2 flux quantum¹⁰. This effect is clearly seen in FIG. 6c, where T_1 is maximal at a phase bias of π , and minimal at a phase bias of 0.

Whereas dissipation at the qubit frequency reduces the T_1 of most conventional qubits that operate at microwave frequencies, quasiparticle dynamics are postulated to result in architecture-specific dephasing owing to a combination of a broad spectrum of low-frequency fluctuations of charge and kinetic inductance. In charge qubits such as the Cooper-pair box, information is encoded in two charge states with even parity that differ in Cooper-pair number by one unit. When a quasiparticle tunnels, the manifold associated with single-charge states is populated, taking the system out of the qubit Hilbert space. Work on single Cooper-pair transistors¹⁰⁶ and Cooper-pair box qubits¹⁰⁷ examined the charge-fluctuation-induced variations of the quantum capacitance of these circuits using microwave reflectometry. The dynamics were consistent with quasiparticle effects¹⁰⁰ and yielded early results on the excess quasiparticle density. Transmon qubits are typically engineered to be relatively insensitive to charge fluctuations and exhibit orders-of-magnitude longer coherence times than Cooper-pair box charge qubits. At the same time, for the purposes of investigating decoherence mechanisms, a weak dependence of the qubit frequency on charge bias can be engineered by adjusting E_j/E_c to correlate fluctuations in parity caused by quasiparticle tunnelling with qubit excitation and relaxation events^{108,109}. In some experiments, an asymmetry in the transition rates biased towards excitation events¹¹⁰ was found to originate in photon-assisted charge parity jumps¹¹¹. Quasiparticles at elevated energies created by these jumps hardly affected the qubit dynamics, unlike in an experiment¹¹² with purposefully injected hot quasiparticles. Quasiparticle sensing can also be achieved with the fluxonium qubit at a flux bias at which the lifetime is dominated by quasiparticle dissipation. Quantum jumps between the qubit states¹¹³ in this regime are dominated by interactions with quasiparticles, and a deviation of the jump statistics away from a Poissonian distribution

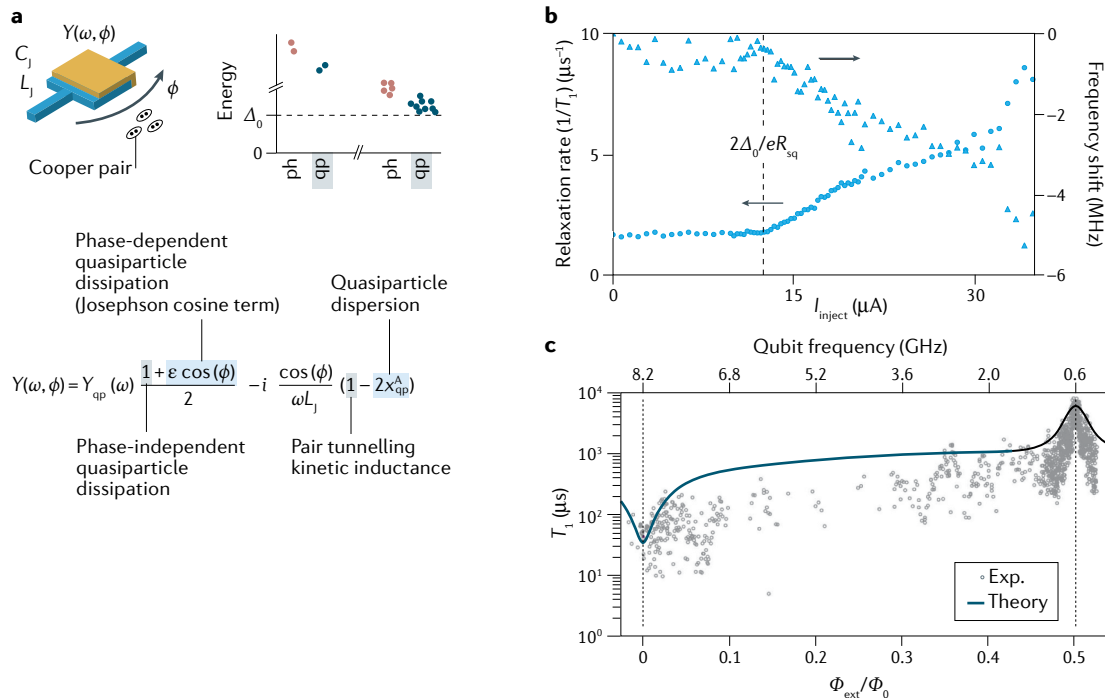


Fig. 6 | Quasiparticles. **a** In the presence of both Cooper-pair and quasiparticle transport, the electrical properties of a junction can be modelled as a complex admittance $Y(\omega, \phi)$. The presence of quasiparticles can result in either dissipation or dispersion via the real and imaginary parts of the admittance, respectively. Quasiparticles can be either free or bound in Andreev states, with normalized densities x_{qp} and x_{qp}^A , respectively. Cooper-pair transport has a dispersive component through the usual kinetic inductance associated with pair tunnelling. Finally, there is a phase-dependent, dissipative term related to the interaction between Cooper pairs and quasiparticles, the ‘Josephson cosine term’. ϵ approaches unity at temperatures well below the superconducting transition temperature. When ionizing radiation with energy greater than the superconducting gap Δ_0 impacts a qubit, many quasiparticles (qp) and phonons (ph) are created, as schematically shown in the graph. These excitations then scatter and relax over time. **b** The dissipative and dispersive effects of quasiparticles are illustrated in phase qubit measurements in which a current I_{inject} is passed across an on-chip SQUID with resistance R_{sq} to produce quasiparticles. A current that produces a voltage equal to the gap ($2\Delta_0/eR_{\text{sq}}$), and thus intense enough to break Cooper pairs, is indicated with a dashed vertical line. **c** The phase-sensitive effect of quasiparticles on the relaxation time T_1 is shown for a fluxonium qubit as a function of the applied magnetic flux Φ_{ext} , measured in units of the flux quantum Φ_0 . ϕ , phase difference across the junction; C , junction capacitance; L , effective inductance. Panel **b** is reprinted with permission from REF.¹⁰², American Physical Society. Panel **c** is adapted from REF.⁴⁰, Springer Nature Limited.

indicates a fluctuation in the quasiparticle population spanning timescales from seconds to hours.

Resonator measurements. Quasiparticle-induced decoherence effects are also seen in high- Q superconducting resonators^{85,114,115}. The presence of quasiparticles can be modelled as a surface admittance, which again has a real part that is dissipative and reduces the resonator Q , and an imaginary part that results in a frequency shift⁸². A decrease in Q reduces the sensitivity of a kinetic inductance detector and can have a trickle-down effect on T_1 when integrated with a qubit. Like in qubits, the quasiparticle density saturates when the resonator operating temperature is reduced, indicating the presence of excess non-equilibrium excitations at temperatures below a few hundred millikelvin¹¹⁶. Stray infrared or high-energy photons can drive pair-breaking events that generate quasiparticles, and this pathway has been linked with the reduction of coherence in many experiments, particularly in studies that systematically probed the role of different levels of infrared and high-energy radiation shielding on resonator Q (REFS^{56,117,118}). In thin-film Al

circuits, microwave reflectometry can probe the complex conductivity of the resonator, and fluctuations therein can be attributed to quasiparticle dynamics⁹⁶. As the resonator is cooled, the quasiparticle recombination time agrees with standard models of electron–phonon scattering down to a few hundred millikelvin, below which a saturation of the lifetime and the extracted number of excess particles is observed; the saturation temperature and density agree with parameters obtained from qubit experiments. The spectrum of quasiparticle fluctuations spans a broad range of values at the low-frequency end of the spectrum.

Trapping structures. With the presence of excess quasiparticles constituting a significant source of decoherence, it is imperative to develop strategies to both mitigate their generation and limit their coupling to qubit structures. Recent work has pointed to high-energy ionizing radiation¹¹⁹, specifically keV muons and MeV gamma rays, as a source of quasiparticles^{11,57}. Such impacts can have correlated noise effects on a group of nearby qubits¹²⁰ and can also fuel a slow cascade of energy

relaxation over long time intervals; these effects are particularly harmful if they create correlated errors that cannot be compensated by quantum error correction¹²¹.

Thus, best practices to improve coherence include increased shielding, which at infrared frequencies involves effective cryopackaging and nested radiation shields. For ionizing radiation, conducting experiments in mines or other locations typically used for high-energy physics experiments has demonstrated improved coherence¹¹⁸. Another approach is to develop traps for both quasiparticles and phonons at the quantum-chip level. Such structures can be based on either microscopic defects or lithographically defined structures. Examples of the former include trapped vortices^{122,123}, which have been shown to be a sink for quasiparticles and result in increased coherence times, and Andreev bound states within a nanowire JJ, which can serve the same function when phase-biased¹²⁴. Engineered structures can incorporate a normal metal¹²⁵ or lower-gap superconductor regions^{97,126,127} to trap quasiparticles, as well as circuits for active pumping using pulses¹²⁸ or voltage-biased tunnel junctions¹²⁹. Traps for phonons can be constructed using absorptive materials¹³⁰ or by harnessing phonon bandgap and bandstop structures originally designed to stop phonon recombination¹³¹.

1/f fluctuations

In the previous sections, we mentioned two specific sources of low-frequency noise: TLS defects and quasiparticles. Types of 1/f noise^{132,133} typically present in quantum circuits include charge fluctuations¹³⁴, magnetic flux noise^{135,136} and fluctuations of the supercurrent in tunnel junctions^{137,138}. Although there is some spread in the intensity, and deviations from a pure 1/f behaviour, of these noise sources from device to device and from one fabrication recipe to another, the mean noise amplitude and frequency spectrum are remarkably universal for a very broad class of circuits.

Background charge noise severely limits coherence in conventional Cooper-pair box type qubits that operate with $E_J/E_C \ll 1$. The transmon qubit was designed to mitigate this noise source¹³⁹. Flux-based qubits operate with a large shunting capacitor or in a regime where charge is highly delocalized, rendering phase a good quantum number and obtaining immunity to charge fluctuations. However, operating in this regime leads to sensitivity to magnetic fluctuations. Flux noise is common to all qubits that use a loop for magnetic bias and can limit coherence: one typically operates at a point of degeneracy where the energy is insensitive to flux to leading order or settles for fixed-frequency qubits. This noise is remarkable, spanning more than 13 orders of magnitude from mHz to 10 GHz, even at low temperatures at which one may expect certain energetic processes to freeze out. Critical current noise is currently the least deleterious of noise sources, especially for submicrometre junctions, and will likely limit dephasing times when the coherence time will exceed milliseconds¹⁴⁰.

Despite many years of intense research, the precise mechanism of 1/f noise remains elusive. A simple theoretical model that produces 1/f noise¹⁴¹ can be obtained by considering hopping between two wells of a double-well

potential over a characteristic time τ . The spectrum of this random telegraph signal at frequency f is $\propto \frac{\tau}{1 + (2\pi f\tau)^2}$. Assuming a distribution of barrier heights for the hopping process yields 1/f-type behaviour at low frequencies. For charge noise and critical current noise, most models envisage some type of electronic traps that arise from structural disorder. In the case of critical current noise, one imagines that tunnelling electrons are trapped for varying periods of time. Flux noise has recently been the subject of intense research that has implicated clusters of spins on metal surfaces with fluctuating magnetic moments. Many scenarios¹⁴² are discussed, but two recent examples attribute such surface spins to trapping in shallow potentials at metal-insulator interfaces¹⁴³ and to surface paramagnetic layers, such as condensed films of molecular oxygen¹³⁵. As materials characterization studies ramp up on superconducting devices, it is an exciting prospect that multimodal structural, characterization and coherence measurements on qubits may shed light on the fundamental origins of low-frequency noise in solids, potentially also clarifying the origin of the flicker noise behaviour observed in many different settings^{141,144}. Moreover, it will be interesting to see if there are connections between the dynamics of TLS defects, quasiparticle dynamics and 1/f fluctuations.

Noise-protected architectures

With an identification of the basic noise sources present in superconducting thin films, resonators and junctions, it is possible to construct qubit architectures that offer varying degrees of immunity to these decoherence processes. One strategy is to make use of ‘clock transitions’, which were developed for atomic clocks. When a qubit is biased at such a transition, the qubit energy, by way of symmetry, is to leading (or perhaps quadratic) order^{145,146} insensitive to fluctuations in a given control parameter; operating at a degeneracy point in external charge or magnetic flux bias is common. Otherwise, one can choose a set of parameters to be made insensitive to a given, intense noise source; the transmon qubit, for example, uses junctions with an E_J/E_C ratio such that the qubit frequency is nearly insensitive to charge noise. Another approach that is now making its way into the laboratory involves storing information in more robust, global degrees of freedom of a qubit circuit, such as a topological invariant of the system. A well-known example involves computing with non-Abelian anyons¹⁴⁷, excitations that exist in a decoherence-free subspace where transitions between the ground and excited states of a qubit can only occur as these exotic particles ‘braid’ or traverse a trajectory around each other, rendering a strong resilience to any local noise source¹⁴⁸. A detailed review by Benoît Douçot and Lev Ioffe provides examples of different noise-protected superconducting circuits²⁵.

Generally speaking, to achieve topological protection, one seeks a circuit where the Hamiltonian can be decomposed into two local subspaces that are mutually orthogonal and do not couple under the action of local operations in either sector. The qubit logical states can then be encoded in the ground states of each isolated subspace, and an energy gap can prevent excitation to higher states within each isolated subsystem. From a

practical standpoint, the realization of such a circuit presents a challenge, because the values of E_J and E_C cannot both be increased simultaneously. This is often desirable to engineer a large excitation gap, and in fact their product is bound by the superconducting gap. Thus, choosing values of these parameters that both enable the observation of quantum dynamics and a sizable excitation gap, especially with Al junctions, is challenging. Another challenge is to construct circuits that are robust to both relaxation and dephasing. Quantum mechanically, this implies that a structure is robust to phase flips and conserves excitation number, quantities that are conjugate pairs. For example, in the 0– π qubits discussed below, one has to suppress phase flips from 0 to π while conserving Cooper-pair parity. When working with pairs of fluxons, the dual quantities are the flux parity and quasiparticle number. Crucially, one must then finally construct global operations that can drive transitions between the qubit states and generate entanglement between qubits, a highly non-trivial design task in a qubit designed to resist all forms of coupling to the external environment.

0– π qubits

Several noise-protected qubit variants have recently been proposed using so-called 0– π circuits^{149–152}, where the usual 2 π periodicity in the phase drop across a single

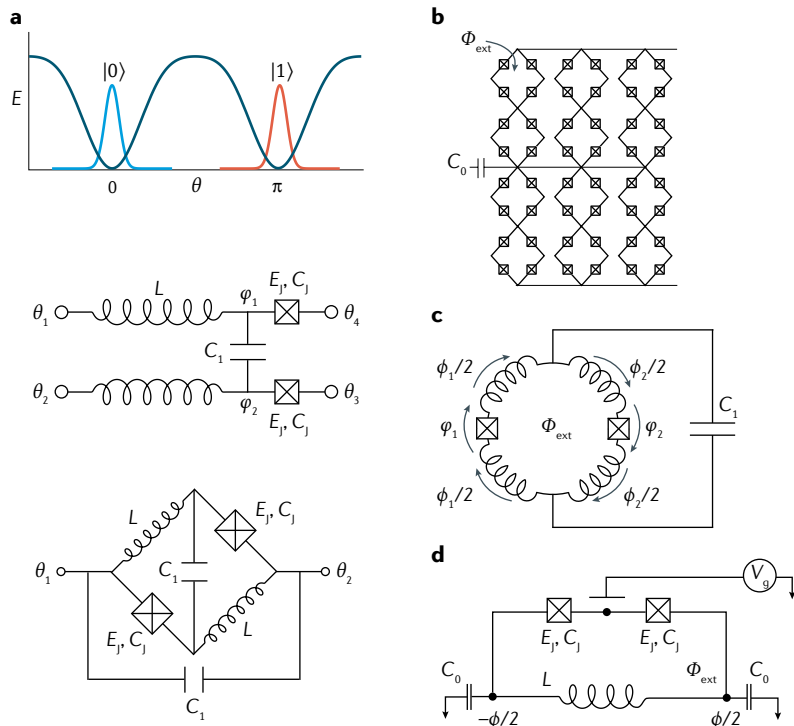


Fig. 7 | Noise-protected circuits. Multiple Josephson junctions can be combined with passive reactive elements to create noise-protected qubits. **a** | Current-mirror implementation of a 0– π qubit that resembles a Wheatstone bridge circuit. **b** | A protected qubit formed by a chain of superconducting rhombi. **c** | A transmon-like protected qubit. **d** | A bifluxon qubit. θ_1 and θ_2 , superconducting phases; ϕ , junction phase drop; ϕ_1 and ϕ_2 , inductor phase drops; Φ_{ext} , external magnetic flux; C_0 , gate capacitance C_1 , shunt capacitance; C_J , junction capacitance; L , inductance. Panel **a** is reprinted with permission from REF.¹⁴⁹, American Physical Society. Panel **b** is adapted from REF.¹⁶¹, Springer Nature Limited. Panel **c** is reprinted from REF.¹⁶⁴, CC BY 4.0. Panel **d** is reprinted from REF.¹⁶⁵, CC BY 4.0.

junction is transformed into a π periodicity in a more complex circuit with several junctions. In such a structure, transport only involves the motion of $4e$ charges (pairs of Copper pairs). The dual of these circuits can also be realized with 4π periodicity and favour the transport of pairs of fluxons. An illustrative example that demonstrates the essential features of these types of circuits is the current-mirror-based 0– π qubit architecture¹⁵³ (FIG. 7a). Consider a parallel chain of JJs connected by capacitive links. The mechanical analogue of the capacitance in these circuits is a mass in an oscillator, and if the external capacitance $C \gg C_J$ in the current mirror, then excitons that carry charge $+2e$ in one rail and $-2e$ in the other rail are lower in energy than individual $\pm 2e$ excitations, that is, processes that change the total charge of an individual branch between the rails. The chain is effectively superconducting along the rails and insulating between them. We can characterize the transport across this chain in terms of the phase difference between the top and bottom of the structure $\phi_{top} - \phi_{bottom}$, where $\phi_{top} = \theta_4 - \theta_1$ and $\phi_{bottom} = \theta_3 - \theta_2$ are expressed in terms of the phases of the four terminals $\theta_1, \theta_2, \theta_3$ and θ_4 . The energy of the circuit would then be a function of this phase difference $E(\phi_{top} - \phi_{bottom})$ and other terms would correspond to $\pm 2e$ excitations across the rails, which are strongly suppressed. If we now fold this four-terminal circuit into a two-terminal one, connecting port 1 to 3 and port 2 to 4, the resulting device has an energy $E(2(\theta_1 - \theta_2))$, which produces the desired minima at a phase difference of 0 and π . Using this basic scheme leads to the circuit shown in FIG. 7a, where external inductances are used to reach the dynamical regime described above, and a large shunting capacitor is used to prevent tunnelling events between these minima. The parameter values of the circuit elements needed to reach this operating regime are challenging to implement experimentally, particularly the inductances, which need to have higher impedance than the resistance quantum. Such ‘superinductors’^{154,155} have an impedance at the frequency of the qubit circuit, typically in the GHz range, that is larger than $h/(2e)^2 \approx 6.5 \text{ k}\Omega$, significantly larger than the 377Ω value characteristic of free space. Recipes to fabricate these elements include using a series array of small tunnelling junctions¹⁵⁶, nanowires¹⁵⁷ or highly disordered superconductors^{158–160} with a large kinetic inductance, such as granular aluminium.

Other circuits with π and 4π periodicity

Additional superconducting circuits with a π -periodic energy functional have also been proposed. A well studied example consists of an array of rhombi^{161,162}, each with four JJs, or two junctions and two inductors, separated by four small superconducting islands (FIG. 7b). When an external magnetic field of half a flux quantum threads the loop, the ground state corresponds to clockwise and anticlockwise currents with an energy splitting given by the charging energy of the junction. When this splitting is smaller than the Josephson energy, excitation to higher levels from the doublet is suppressed. Rhombi can be arranged in parallel chains and connected to superconducting wires at each end to form a two-terminal device. In the presence of a finite charging energy, only

tunnelling events that flip an even number of rhombi preserve the ground states of the Hamiltonian, which are now separated by a phase difference of π . Measurements on this qubit are ongoing, with a 100-fold increase in T_1 up to $\sim 70\text{ }\mu\text{s}$ reported in the protected state¹⁶³. More recently, an architecture similar to the transmon but with a π -periodic Josephson element has been proposed¹⁶⁴ (FIG. 7c). This element consists of a loop with two JJs and four inductors where the charge carriers are again pairs of Cooper pairs. Numerical modelling indicates that a high degree of protection against energy relaxation and dephasing is expected for reasonable inductances and junction parameters. Finally, a dual version of these circuits, the bifluxon qubit, can be realized by using a charge qubit formed by two JJs connected via a superconducting island (FIG. 7d). When this island is biased with one-half of a Cooper pair and incorporated into a loop with a large inductance, the Aharonov–Casher effect results in a 4π -periodic surface that preserves the parity of fluxons in the circuit and yields a Hamiltonian that separates into two independent sectors. This structure protects against energy relaxation, and dephasing is inhibited by a preference for double fluxon tunnelling. Recent experiments on this qubit have shown a 10-fold increase in the energy relaxation time up to $\sim 100\text{ }\mu\text{s}$ (REF. ¹⁶⁵).

Although improving materials quality to boost coherence will always be a critical driver for any quantum processor architecture, it is important to quantify what level of perfection is needed to reach a threshold above which coherent lifetimes are sufficiently long to enable quantum error correction. Qubit structures with some degree of noise protection incorporated into the hardware itself promise to achieve fault-tolerant operation with a higher density of materials defects, albeit at the expense of more complex fabrication and gate protocols.

Emerging Josephson devices

The overwhelming majority of qubit circuits so far have used Josephson tunnelling junctions, and specifically devices in which the surface of a polycrystalline Al film is oxidized in a vacuum chamber to grow an oxide layer $\sim 1\text{ nm}$ thick, followed by the in situ deposition of a top Al electrode to complete an Al/AlO_x/Al structure¹⁶⁶. These devices are remarkably robust in terms of fractional yield of working devices, and when placed in circuits with very few wiring elements, such as a transmon in a 3D cavity, can reach coherence times approaching a millisecond. The contribution of the tunnel barrier is probably not the dominant loss mechanism. That being said, these devices work well in an average sense; the thickness and chemical composition of the barrier vary significantly, even in submicrometre junctions. The junction barrier is metastable and the tunnel resistance changes when exposed to air, the edges of the junction are rough, and transport is likely to be dominated by a few high-transparency regions of the junction rather than having a uniform distribution¹⁶⁷. As we move to quantum circuits with larger numbers of qubits and longer-lived coherence, we will require junctions with lower microwave frequency loss, very small fluctuations of the critical current, and robust fabrication recipes that yield less than a per cent of resistance variation over

wafers of devices. There have been many efforts targeting the fabrication of tunnel junctions using different superconductors and oxides that are epitaxially growth- and lattice-matched. For example, a multilayer of Re/Ti can be matched to a sapphire substrate and crystalline Al₂O₃ can be used for the junction barrier^{168,169}. Another option involves using NbN superconductors with an AlN barrier grown on MgO (REF. ¹⁷⁰). These systems have resulted in coherent operation, but fabricating robust structures with long-lived coherence remains elusive. A key element of this technical challenge is that high-transparency tunnel barriers constructed from high-bandgap insulators typically have a relatively small lattice spacing, mandating near-atomic-level control of the barrier thickness to tune the tunnel current over the desired range of parameters.

An approach that potentially circumvents this problem is to form JJs using 2D van der Waals (vdW) quantum materials¹⁷¹, which can exhibit a full range of tunable conductivity from superconducting to insulating. Whereas a diffusive normal conductor is typically not a good choice for a junction barrier on account of its dissipation, ballistic transport is possible in clean graphene; hexagonal boron nitride can be fully insulating; and NbSe₂ is superconducting. Superconducting quantum interference devices (SQUIDS) that can be tuned both with an electrostatic backgate and a magnetic flux have been realized with graphene¹⁷². Recently, coherent oscillations have been obtained in a transmon qubit with a boron nitride/graphene/boron nitride tunnel barrier¹⁷³ (FIG. 8a). These high-quality thin films hold the promise of an scalable fabrication procedure for reproducible, low-defect-density junctions with high-coherence properties, but further design improvements are needed to suppress known decoherence channels that arise, for example, from gating structures. Additionally, more complex vdW heterostructures, for example moiré stacks¹⁷⁴, in which electronic properties are tuned by varying the orientation of adjacent layers in combination with electrostatic gating, can behave as a metal, superconductor, band insulator, Mott insulator or topological Chern insulator. These additional features may enable more complex topological encoding of information and an intrinsic resilience to decoherence. Recent experimental work has demonstrated qubits based on MoS₂ (REF. ¹⁷⁵), MoTe₂ (REF. ¹⁷⁶) and NbSe₂ (REF. ¹⁷⁷) junctions.

Finally, we note that it is possible to create junctions that leverage narrow constrictions rather than planar barriers. Nanobridges that are short (of order the coherence length) and connected to banks that act as superconducting reservoirs¹⁷⁸ can yield a non-linear current–phase relation approaching the ideal value given by the Kulik–Omelyanchuk theory¹⁵: $I(\phi) = \frac{I_0}{2} \cos(\phi/2) \tanh^{-1}(\sin(\phi/2))$. However, even for dimensions achieved with state-of-the-art lithography, the critical current for such devices is tens of microamperes, requiring a shunting capacitor with $C > \text{pF}$ to achieve a qubit frequency in the GHz range. Producing an overlap capacitor with sufficiently low loss to achieve 100s of microseconds of coherence is very challenging, even for some of the best thin-film dielectrics such as a-Si.

One could place two such nanobridge junctions in a loop and use a magnetic field to lower the effective critical current. However, such a phase bias lowers the Andreev bound-state gap in this high-transparency structure, effectively trapping/untrapping quasiparticles and inducing decoherence¹²⁴. Alternatively, one can consider long nanowire devices where transport is dominated by coherent phase slips. Coherent phase slips¹⁷⁹ are the dual of Cooper pairs tunnelling. When a phase-slip element, such as a very thin, narrow and long wire is placed in a loop and magnetically biased at 1/2 flux quantum, degenerate, opposite circulating current states can be stabilized^{180–182} (FIG. 8b). Alternatively, a tunnel-junction-free, charge-insensitive qubit such as a transmon can be realized using granular aluminium as a nonlinear element¹⁸³.

Outlook

The design of materials systems that enable the production, preservation and processing of quantum entanglement is a critical step in the realization of quantum information processing technologies. A summary of the main sources of decoherence in state-of-the-art qubits and current mitigation strategies is presented in TABLE 1. In crystals of highly correlated quantum materials, nature preserves coherence through symmetry and structural perfection, protecting individual constituents from local perturbation and expressing the signatures of the underlying quantum mechanics only in ensemble properties. For quantum information processing, the challenge is to synthesize matter with a high degree of coherence, programmable entanglement of varying complexity, and open communication channels to control and measure each individual quantum system. Constructing quantum information systems is a co-design process that involves balancing architecture, materials development and control.

In one limit, simple architectures allow efficient coupling to the external environment and a variety of accessible gate operations and error-mitigation strategies. Perfection in this case is placed in the quality of

materials needed to prepare qubits. In another limit, greater complexity can be placed in the architecture by encoding information in delocalized quantities, increasing the resilience towards local noise sources, but mandating more complex fabrication and logical operation. Such topological protection can be achieved using more elaborate circuits with multiple JJs or potentially using basic materials that can preserve quantum coherence in protected internal degrees of freedom. The challenge in either approach is to decouple decoherence channels while permitting quantum control.

Conventional qubit architectures are limited by TLS defects, non-equilibrium quasiparticles and 1/f flux noise. Although tremendous progress has been made in different types of theoretical models describing TLS defects, a major outstanding challenge remains the pairing of theory with definitive experiments to confirm the identity and dynamics of these defects and their dominant coupling mechanism to quantum circuits. Included in this pursuit is the determination of the relative contributions of coherent, incoherent and ensemble TLS dynamics on qubit coherence times and their fluctuations. Furthermore, developing simple materials characterization recipes to quantify the presence of confirmed, decoherence-inducing TLS defects that serve as a proxy in lieu of full cryogenic characterization will be a tremendous step forward in accelerating the development of robust materials with high quantum coherence. With respect to quasiparticles, in addition to trapping these excitations in normal metal structures, acoustic engineering may be a very effective mitigation strategy. Fundamental calculations and experiments to identify the specific phonon frequencies that are deleterious to quantum circuit operation would be valuable in guiding the design of appropriate filtering structures, as it is difficult to block a broadband set of excitations that range in frequency from Hz to THz. Also, one does not want to decouple any channels needed for thermalization of the quantum circuit.

Noise protection can also be achieved by using qubit designs that spread information across delocalized

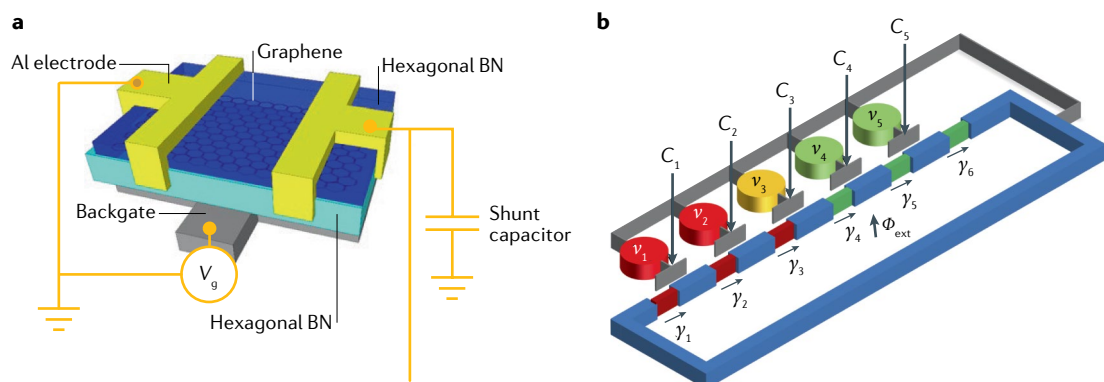


Fig. 8 | Novel superconducting qubits. **a** | Voltage-tunable 2D van der Waals heterostructures can be used to realize gated Josephson junctions, potentially resulting in improved fabrication uniformity and noise-protected encoding of quantum information. **b** | Qubits based on nanowire constrictions can be formed by controlling coherent phase slips, which are dual excitations to the usual tunnelling of Cooper pairs. Each constriction is voltage-biased with intensity v_n via a capacitance C_n . The phase drop across each link is γ_n . The loop can be biased with an external magnetic flux Φ_{ext} . Panel **a** is adapted from REF.¹⁷³, Springer Nature Limited. Panel **b** is reprinted with permission from REF.¹⁸¹, American Physical Society.

Table 1 | Summary of key decoherence mechanisms, their origin and possible mitigation strategies

Noise source	Origin	Decoherence channel	Mitigation strategy
Two-level system (TLS) defects	Lack of crystalline order in amorphous films that creates a glass-like system characterized by quantum tunnelling between two energy minima, possibly representing similar configurations of individual atoms, atomic clusters and electronic states	Individual TLS defects with long-lived coherence and resonant with a qubit cause energy relaxation. Ensembles of fluctuating TLS defects contribute to dephasing, and TLS-TLS interactions can result in slow drifts of qubit coherence times	Etching and passivation to remove amorphous layers; use of crystalline dielectrics and ordered Josephson junction barriers. The underlying microscopic mechanisms need to be identified
Quasiparticles and phonons	Incident ionizing radiation that breaks Cooper pairs, generating highly excited quasiparticles and phonons that scatter away energy in a multistep cascade with a complex noise spectrum	Dissipation at microwave frequencies and dispersive shifts and/or fluctuations of the qubit frequency, which result in dephasing	Normal metal/low-gap superconducting traps to remove quasiparticles from the qubit area; acoustic absorbers and frequency-tailored structures to suppress phonon propagation and secondary pair breaking
1/f magnetic flux noise	Spins or clusters of spins on metallic surfaces, potentially resulting from magnetic defects, electrons trapped in disorder potentials, or paramagnetic films that condense at low temperatures	A broad 1/f-type noise spectrum contributing to dephasing in circuits with a superconducting loop and operated away from flux degeneracy	Initial work indicates noise reduction with capping layers. Need to identify precisely the microscopic origin to develop robust, tailored elimination strategies

modes of a Josephson circuit. These designs are attractive because one may achieve higher-fidelity quantum operations in the presence of higher levels of localized noise sources and fluctuations. At the same time, these architectures typically require the fabrication of more complex circuit elements such as superconductors and qubits with a high degree of symmetry in the circuit, pushing current junction fabrication technology to new limits to achieve near-identical parameter values. Specifically, with superinductors, a main challenge is to minimize parasitic capacitance. Devices leveraging suspended metallic films, disordered materials such as granular aluminium and thin films of niobium alloys, and junction arrays have started to open up this frontier of new qubit devices, and the space is ripe for innovation with respect to both materials optimization and new fabrication approaches.

In summary, boosting coherence in superconducting circuits defines a wide tradespace of materials research, encompassing high-quality insulators, low-loss superconducting metals and new JJs. For insulating materials, the wish-list includes structures that have less than 1 ppm loss at microwave frequencies and 10–100 times lower 1/f noise than currently observed, particularly magnetic flux noise when leveraging charge-insensitive

qubit designs. Expanding our toolbox of superconducting metals and the substrates on which they can be grown, and integrating them with sinks for non-equilibrium excitations are key to engineering a resilience to quasiparticle loss. Finally, continued progress in junction development is needed to improve the uniformity of JJs, the functionality of JJs using more complex barrier materials, and to develop phase-slip devices; these advances will open up a new frontier of superconducting circuits, including devices with more complete noise protection.

The backbone of all of these advanced materials is the seamless integration of sophisticated materials characterization techniques to benchmark expected coherence levels throughout the fabrication process and to maintain quality control. Developing robust and simple proxy measurements with standard metrics to predict qubit properties will help to nucleate technological breakthroughs across all quantum processor architectures. It will also shed light on the fundamental noise mechanisms present in solid-state systems, bringing resolution to many unsolved mysteries while exploring quantum mechanics at the complexity frontier.

Published online 23 September 2021

1. Nielsen, M. A. & Chuang, I. L. *Quantum Computation and Quantum Information* 10th anniversary edn (Cambridge Univ. Press, 2010).
2. Hidary, J. D. *Quantum Computing: An Applied Approach* (Springer, 2019).
3. Bell, J. S. & Aspect, A. *Speakable and Unspeakable in Quantum Mechanics. Collected Papers on Quantum Philosophy* (Cambridge Univ. Press, 2008).
4. Zurek, W. H. Decoherence and the transition from quantum to classical. *Phys. Today* **44**, 36–44 (1991).
5. Terhal, B. M. Quantum error correction for quantum memories. *Rev. Mod. Phys.* **87**, 307–346 (2015).
6. Arute, F. et al. Quantum supremacy using a programmable superconducting processor. *Nature* **574**, 505–510 (2019).
7. Devoret, M. H. & Schoelkopf, R. J. Superconducting circuits for quantum information: an outlook. *Science* **339**, 1169–1174 (2013).
8. Nakamura, Y., Pashkin, Y. A. & Tsai, J. S. Coherent control of macroscopic quantum states in a single-Cooper-pair box. *Nature* **398**, 786–788 (1999).
9. Tinkham, M. *Introduction to Superconductivity* 2nd edn (Dover, 2004).
10. Martinis, J. M., Devoret, M. H. & Clarke, J. Energy-level quantization in the zero-voltage state of a current-biased Josephson junction. *Phys. Rev. Lett.* **55**, 1543–1546 (1985).
11. Martinis, J. M., Devoret, M. H. & Clarke, J. Quantum Josephson junction circuits and the dawn of artificial atoms. *Nat. Phys.* **16**, 234–237 (2020).
12. Koch, J. et al. Charge-insensitive qubit design derived from the Cooper pair box. *Phys. Rev. A* **76**, 042319 (2007).
13. You, J. Q., Hu, X., Ashhab, S. & Nori, F. Low-decoherence flux qubit. *Phys. Rev. B* **75**, 140515 (2007).
14. Duzer, T. V. *Principles of Superconductive Devices and Circuits* 2nd edn (Prentice Hall, 1998).
15. Golubov, A. A., Kupriyanov, M. Y. & Il'ichev, E. The current-phase relation in Josephson junctions. *Rev. Mod. Phys.* **76**, 411–469 (2004).
16. Makhlin, Y., Schön, G. & Shnirman, A. Quantum-state engineering with Josephson-junction devices. *Rev. Mod. Phys.* **73**, 357–400 (2001).
17. Wendin, G. & Shumeiko, V. S. Quantum bits with Josephson junctions (review article). *Low Temp. Phys.* **33**, 724–744 (2007).
18. Kjaergaard, M. et al. Superconducting qubits: current state of play. *Annu. Rev. Condens. Matter Phys.* **11**, 369–395 (2020).
19. Krantz, P. et al. A quantum engineers guide to superconducting qubits. *Appl. Phys. Rev.* **6**, 021318 (2019).
20. Wendin, G. Quantum information processing with superconducting circuits: a review. *Rep. Prog. Phys.* **80**, 106001 (2017).
21. Kockum, A. F. & Nori, F. In *Fundamentals and Frontiers of the Josephson Effect* (ed. Tafuri, F.) 703–741 (Springer, 2019).
22. Wang, C. et al. Surface participation and dielectric loss in superconducting qubits. *Appl. Phys. Lett.* **107**, 162601 (2015).
23. Córcoles, A. D. et al. Protecting superconducting qubits from radiation. *Appl. Phys. Lett.* **99**, 181906 (2011).
24. Gambetta, J. M. et al. Investigating surface loss effects in superconducting transmon qubits. *IEEE Trans. Appl. Superconductivity* **27**, 1–5 (2017).
25. Douçot, B. & Ioffe, L. B. Physical implementation of protected qubits. *Rep. Prog. Phys.* **75**, 072001 (2012).

26. Esteve, D., Devoret, M. H. & Martinis, J. M. Effect of an arbitrary dissipative circuit on the quantum energy levels and tunneling of a Josephson junction. *Phys. Rev. B* **34**, 158–163 (1986).
27. Oliver, W. D. & Welander, P. B. Materials in superconducting quantum bits. *MRS Bull.* **38**, 816–825 (2013).
28. Müller, C., Cole, J. H. & Lisenfeld, J. Towards understanding two-level-systems in amorphous solids: insights from quantum circuits. *Rep. Prog. Phys.* **82**, 124501 (2019).
29. Arutyunov, K. Y. et al. Relaxation of nonequilibrium quasiparticles in mesoscopic size superconductors. *J. Phys. Condens. Matter* **30**, 343001 (2018).
30. Glazman, L. I. & Catelani, G. Bogoliubov quasiparticles in superconducting qubits. *SciPost Phys. Lect. Notes* <https://doi.org/10.21468/SciPostPhysLectNotes.31> (2021).
31. Devoret, M., Huard, B., Schoelkopf, R. & Cugliandolo, L. F. (eds) *Quantum Machines: Measurement and Control of Engineered Quantum Systems* Vol. 96 (Oxford Univ. Press, 2014).
32. Gokhale, P. et al. Extending the frontier of quantum computers with qutrits. *IEEE Micro* **40**, 64–72 (2020).
33. Morvan, A. et al. Outfit randomized benchmarking. *Phys. Rev. Lett.* **126**, 210504 (2021).
34. Kreikebaum, J. M., O'Brien, K. P., Morvan, A. & Siddiqi, I. Improving wafer-scale Josephson junction resistance variation in superconducting quantum coherent circuits. *Supercond. Sci. Technol.* **33**, 06LT02 (2020).
35. Martinis, J. M., Nam, S., Aumentado, J. & Urbina, C. Rabi oscillations in a large Josephson-junction qubit. *Phys. Rev. Lett.* **89**, 117901 (2002).
36. Steffen, M. et al. State tomography of capacitively shunted phase qubits with high fidelity. *Phys. Rev. Lett.* **97**, 050502 (2006).
37. Paik, H. et al. Observation of high coherence in Josephson junction qubits measured in a three-dimensional circuit QED architecture. *Phys. Rev. Lett.* **107**, 240501 (2011).
38. Mooij, J. E. et al. Josephson persistent-current qubit. *Science* **285**, 1036–1039 (1999).
39. Manucharyan, V. E., Koch, J., Glazman, L. I. & Devoret, M. H. Fluxonium: single Cooper-pair circuit free of charge offsets. *Science* **326**, 113–116 (2009).
40. Pop, I. M. et al. Coherent suppression of electromagnetic dissipation due to superconducting quasiparticles. *Nature* **508**, 369–372 (2014).
41. Nguyen, L. B. et al. High-coherence fluxonium qubit. *Phys. Rev. X* **9**, 041041 (2019).
42. Earnest, N. et al. Realization of a Λ system with metastable states of a capacitively shunted fluxonium. *Phys. Rev. Lett.* **120**, 150504 (2018).
43. Wallraff, A. et al. Strong coupling of a single photon to a superconducting qubit using circuit quantum electrodynamics. *Nature* **431**, 162–167 (2004).
44. Göppel, M. et al. Coplanar waveguide resonators for circuit quantum electrodynamics. *J. Appl. Phys.* **104**, 113904 (2008).
45. Blais, A., Huang, R.-S., Wallraff, A., Girvin, S. M. & Schoelkopf, R. J. Cavity quantum electrodynamics for superconducting electrical circuits: an architecture for quantum computation. *Phys. Rev. A* **69**, 062320 (2004).
46. Mirrahimi, M. et al. Dynamically protected cat-qubits: a new paradigm for universal quantum computation. *N. J. Phys.* **16**, 045014 (2014).
47. Rosenberg, D. et al. 3D integrated superconducting qubits. *npj Quantum Inf.* **3**, 42 (2017).
48. Brecht, T. et al. Demonstration of superconducting micromachined cavities. *Appl. Phys. Lett.* **107**, 192603 (2015).
49. Minev, Z. K. et al. Planar multilayer circuit quantum electrodynamics. *Phys. Rev. Appl.* **5**, 044021 (2016).
50. O'Connell, A. D. et al. Microwave dielectric loss at single photon energies and millikelvin temperatures. *Appl. Phys. Lett.* **92**, 112903 (2008).
51. Kaiser, C. et al. Measurement of dielectric losses in amorphous thin films at gigahertz frequencies using superconducting resonators. *Supercond. Sci. Technol.* **23**, 075008 (2010).
52. Sarabi, B., Ramanayaka, A. N., Burin, A. L., Wellstood, F. C. & Osborn, K. D. Projected dipole moments of individual two-level defects extracted using circuit quantum electrodynamics. *Phys. Rev. Lett.* **116**, 167002 (2016).
53. Pappas, D. P., Vissers, M. R., Wisbey, D. S., Kline, J. S. & Gao, J. Two level system loss in superconducting microwave resonators. *IEEE Trans. Appl. Supercond.* **21**, 871–874 (2011).
54. Faoro, L. & Ioffe, L. B. Internal loss of superconducting resonators induced by interacting two-level systems. *Phys. Rev. Lett.* **109**, 157005 (2012).
55. Faoro, L. & Ioffe, L. B. Interacting tunneling model for two-level systems in amorphous materials and its predictions for their dephasing and noise in superconducting microresonators. *Phys. Rev. B* **91**, 014201 (2015).
56. Barends, R. et al. Minimizing quasiparticle generation from stray infrared light in superconducting quantum circuits. *Appl. Phys. Lett.* **99**, 113507 (2011).
57. Vepsäläinen, A. P. et al. Impact of ionizing radiation on superconducting qubit coherence. *Nature* **584**, 551–556 (2020).
58. Cohen-Tannoudji, C., Dupont-Roc, J. & Grynberg, G. *Atom-Photon Interactions: Basic Processes and Applications* (Wiley, 1992).
59. Anderson, P. W., Halperin, B. I. & Varma, C. M. Anomalous low-temperature thermal properties of glasses and spin glasses. *Phil. Mag.* **25**, 1–9 (1972).
60. Phillips, W. A. Two-level states in glasses. *Rep. Prog. Phys.* **50**, 1657–1708 (1987).
61. Phillips, W. A. Tunneling states in amorphous solids. *J. Low Temp. Phys.* **7**, 351–360 (1972).
62. Dekker, H. Quantum mechanical barrier problems: III. Dissipative tunnelling at finite temperatures for the weakly biased oscillator. *Phys. A* **146**, 396–403 (1987).
63. Halataei, S. M. H. & Leggett, A. J. Tunnel splitting in asymmetric double well potentials: an improved WKB calculation (Univ. Illinois, 2017).
64. Ku, L.-C. & Yu, C. C. Decoherence of a Josephson qubit due to coupling to two-level systems. *Phys. Rev. B* **72**, 024526 (2005).
65. Steffen, M., Sandberg, M. & Srinivasan, S. Recent research trends for high coherence quantum circuits. *Supercond. Sci. Technol.* **30**, 030301 (2017).
66. Burnett, J. J. et al. Decoherence benchmarking of superconducting qubits. *npj Quantum Inf.* **5**, 54 (2019).
67. Shnirman, A., Schön, G., Martin, I. & Makhlin, Y. Low- and high-frequency noise from coherent two-level systems. *Phys. Rev. Lett.* **94**, 127002 (2005).
68. Simmonds, R. W. et al. Decoherence in Josephson phase qubits from junction resonators. *Phys. Rev. Lett.* **93**, 077003 (2004).
69. Martinis, J. M. et al. Decoherence in Josephson qubits from dielectric loss. *Phys. Rev. Lett.* **95**, 210503 (2005).
70. Simmonds, R. W. et al. Coherent interactions between phase qubits, cavities, and TLS defects. *Quantum Inf. Process.* **8**, 117–131 (2009).
71. Gunnarsson, D. et al. Dielectric losses in multi-layer Josephson junction qubits. *Supercond. Sci. Technol.* **26**, 085010 (2013).
72. Palomaki, T. A. et al. Multilevel spectroscopy of two-level systems coupled to a dc SQUID phase qubit. *Phys. Rev. B* **81**, 144503 (2010).
73. Barends, R. et al. Coherent Josephson qubit suitable for scalable quantum integrated circuits. *Phys. Rev. Lett.* **111**, 080502 (2013).
74. Paladino, E., Galperin, Y. M., Falci, G. & Altshuler, B. L. 1/f noise: implications for solid-state quantum information. *Rev. Mod. Phys.* **86**, 361–418 (2014).
75. Müller, C., Lisenfeld, J., Shnirman, A. & Poletto, S. Interacting two-level defects as sources of fluctuating high-frequency noise in superconducting circuits. *Phys. Rev. B* **92**, 035442 (2015).
76. Schlör, S. et al. Correlating decoherence in transmon qubits: low frequency noise by single fluctuators. *Phys. Rev. Lett.* **123**, 190502 (2019).
77. Klimov, P. V. et al. Fluctuations of energy-relaxation times in superconducting qubits. *Phys. Rev. Lett.* **121**, 090502 (2018).
78. Grabovskij, G. J., Peichl, T., Lisenfeld, J., Weiss, G. & Ustinov, A. V. Strain tuning of individual atomic tunneling systems detected by a superconducting qubit. *Science* **358**, 232–234 (2012).
79. Lisenfeld, J. et al. Electric field spectroscopy of material defects in transmon qubits. *npj Quantum Inf.* **5**, 105 (2019).
80. Lisenfeld, J. et al. Observation of directly interacting coherent two-level systems in an amorphous material. *Nat. Commun.* **6**, 6182 (2015).
81. Zmuidzinas, J. Superconducting microresonators: physics and applications. *Annu. Rev. Condens. Matter Phys.* **3**, 169–214 (2012).
82. McRae, C. R. H. et al. Materials loss measurements using superconducting microwave resonators. *Rev. Sci. Instrum.* **91**, 91101 (2020).
83. Day, P. K., LeDuc, H. G., Mazin, B. A., Vayonakis, A. & Zmuidzinas, J. A broadband superconducting detector suitable for use in large arrays. *Nature* **425**, 817–821 (2003).
84. Gao, J. *The Physics of Superconducting Microwave Resonators*. Thesis, Calif. Inst. Technol. (2008).
85. Burnett, J., Bengtsson, A., Niepce, D. & Bylander, J. Noise and loss of superconducting aluminium resonators at single photon energies. *J. Phys. Conf. Ser.* **969**, 012131 (2018).
86. Wang, H. et al. Improving the coherence time of superconducting coplanar resonators. *Appl. Phys. Lett.* **95**, 233508 (2009).
87. Khalil, M. S. et al. Landau-Zener population control and dipole measurement of a two-level-system bath. *Phys. Rev. B* **90**, 100201 (2014).
88. Paik, H. & Osborn, K. D. Reducing quantum-regime dielectric loss of silicon nitride for superconducting quantum circuits. *Appl. Phys. Lett.* **96**, 072505 (2010).
89. Altoé, M. V. P. et al. Localization and reduction of superconducting quantum coherent circuit losses. Preprint at [arXiv https://arxiv.org/abs/2012.07604](https://arxiv.org/abs/2012.07604) (2020).
90. Verjauw, J. et al. Investigation of microwave loss induced by oxide regrowth in high-Q niobium resonators. *Phys. Rev. Appl.* **16**, 014018 (2021).
91. Noroozian, O. et al. Two-level system noise reduction for microwave kinetic inductance detectors. *AIP Conf. Proc.* **1185**, 148–151 (2009).
92. Gao, J. et al. Power dependence of phase noise in microwave kinetic inductance detectors. *Proc. SPIE* **6275**, 64–71 (2006).
93. de Graaf, S. E. et al. Two-level systems in superconducting quantum devices due to trapped quasiparticles. *Sci. Adv.* **6**, eabc5055 (2020).
94. Place, A. P. M. et al. New material platform for superconducting transmon qubits with coherence times exceeding 0.3 milliseconds. *Nat. Commun.* **12**, 1779 (2020).
95. Romanenko, A. et al. Three-dimensional superconducting resonators at $T < 20\text{ mK}$ with photon lifetimes up to $\tau = 2\text{ s}$. *Phys. Rev. Appl.* **13**, 034032 (2020).
96. de Visser, P. J. et al. Number fluctuations of sparse quasiparticles in a superconductor. *Phys. Rev. Lett.* **106**, 167004 (2011).
97. Martinis, J. M. Saving superconducting quantum processors from decay and correlated errors generated by gamma and cosmic rays. *npj Quantum Inf.* **7**, 90 (2021).
98. Mattis, D. C. & Bardeen, J. Theory of the anomalous skin effect in normal and superconducting metals. *Phys. Rev.* **111**, 412–417 (1958).
99. Annett, J. F. & Kruchinin, S. (eds) *New Trends in Superconductivity* (Kluwer, 2002).
100. Martinis, J. M., Ansmann, M. & Aumentado, J. Energy decay in superconducting Josephson-junction qubits from nonequilibrium quasiparticle excitations. *Phys. Rev. Lett.* **103**, 097002 (2009).
101. Catelani, G. & Basko, D. Non-equilibrium quasiparticles in superconducting circuits: photons vs. phonons. *SciPost Phys.* **6**, 013 (2019).
102. Lenander, M. et al. Measurement of energy decay in superconducting qubits from nonequilibrium quasiparticles. *Phys. Rev. B* **84**, 024501 (2011).
103. Catelani, G., Nigg, S. E., Girvin, S. M., Schoelkopf, R. J. & Glazman, L. I. Decoherence of superconducting qubits caused by quasiparticle tunneling. *Phys. Rev. B* **86**, 184514 (2012).
104. Catelani, G., Schoelkopf, R. J., Devoret, M. H. & Glazman, L. I. Relaxation and frequency shifts induced by quasiparticles in superconducting qubits. *Phys. Rev. B* **84**, 064517 (2011).
105. Catelani, G. et al. Quasiparticle relaxation of superconducting qubits in the presence of flux. *Phys. Rev. Lett.* **106**, 077002 (2011).
106. Naaman, O. & Aumentado, J. Time-domain measurements of quasiparticle tunneling rates in a single-Cooper-pair transistor. *Phys. Rev. B* **73**, 172504 (2006).
107. Shaw, M. D., Lutchyn, R. M., Delsing, P. & Echternach, P. M. Kinetics of nonequilibrium quasiparticle tunneling in superconducting charge qubits. *Phys. Rev. B* **78**, 024503 (2008).
108. Ristè, D. et al. Millisecond charge-parity fluctuations and induced decoherence in a superconducting transmon qubit. *Nat. Commun.* **4**, 1913 (2013).
109. Sun, L. et al. Measurements of quasiparticle tunneling dynamics in a band-gap-engineered transmon qubit. *Phys. Rev. Lett.* **108**, 230509 (2012).
110. Serniak, K. et al. Hot nonequilibrium quasiparticles in transmon qubits. *Phys. Rev. Lett.* **121**, 157701 (2018).

111. Houzet, M., Serniak, K., Catelani, G., Devoret, M. H. & Glazman, L. I. Photon-assisted charge-parity jumps in a superconducting qubit. *Phys. Rev. Lett.* **123**, 107704 (2019).
112. Wenner, J. et al. Excitation of superconducting qubits from hot nonequilibrium quasiparticles. *Phys. Rev. Lett.* **110**, 150502 (2013).
113. Vool, U. et al. Non-poissonian quantum jumps of a fluxonium qubit due to quasiparticle excitations. *Phys. Rev. Lett.* **113**, 247001 (2014).
114. Grünhaupt, L. et al. Loss mechanisms and quasiparticle dynamics in superconducting microwave resonators made of thin-film granular aluminum. *Phys. Rev. Lett.* **121**, 117001 (2018).
115. Goetz, J. et al. Loss mechanisms in superconducting thin film microwave resonators. *J. Appl. Phys.* **119**, 015304 (2016).
116. de Visser, P. J. et al. Evidence of a nonequilibrium distribution of quasiparticles in the microwave response of a superconducting aluminum resonator. *Phys. Rev. Lett.* **112**, 047004 (2014).
117. Kreikebaum, J. M., Dove, A., Livingston, W., Kim, E. & Siddiqi, I. Optimization of infrared and magnetic shielding of superconducting TiN and Al coplanar microwave resonators. *Supercond. Sci. Technol.* **29**, 104002 (2016).
118. Cardani, L. et al. Reducing the impact of radioactivity on quantum circuits in a deep-underground facility. *Nat. Commun.* **12**, 2733 (2021).
119. Swenson, L. J. et al. High-speed phonon imaging using frequency-multiplexed kinetic inductance detectors. *Appl. Phys. Lett.* **96**, 263511 (2010).
120. Wilén, C. D. et al. Correlated charge noise and relaxation errors in superconducting qubits. *Nature* **594**, 369–373 (2021).
121. McEwen, M. et al. Resolving catastrophic error bursts from cosmic rays in large arrays of superconducting qubits. Preprint at [arXiv](https://arxiv.org/abs/2104.05219) [https://arxiv.org/abs/2104.05219] (2021).
122. Taupin, M., Khaymovich, I. M., Meschke, M., Mel'nikov, A. S. & Pekola, J. P. Tunable quasiparticle trapping in Meissner and vortex states of mesoscopic superconductors. *Nat. Commun.* **7**, 10977 (2016).
123. Wang, C. et al. Measurement and control of quasiparticle dynamics in a superconducting qubit. *Nat. Commun.* **5**, 5836 (2014).
124. Levenson-Falk, E. M., Kos, F., Vijay, R., Glazman, L. & Siddiqi, I. Single-quasiparticle trapping in aluminum nanobridge Josephson junctions. *Phys. Rev. Lett.* **112**, 047002 (2014).
125. Riwar, R.-P. et al. Normal-metal quasiparticle traps for superconducting qubits. *Phys. Rev. B* **94**, 104516 (2016).
126. Aumentado, J., Keller, M. W., Martinis, J. M. & Devoret, M. H. Nonequilibrium quasiparticles and 2e periodicity in single-Cooper-pair transistors. *Phys. Rev. Lett.* **92**, 066802 (2004).
127. Riwar, R.-P. & Catelani, G. Efficient quasiparticle traps with low dissipation through gap engineering. *Phys. Rev. B* **100**, 144514 (2019).
128. Gustavsson, S. et al. Suppressing relaxation in superconducting qubits by quasiparticle pumping. *Science* **354**, 1573–1577 (2016).
129. Marín-Suárez, M., Peltonen, J. T. & Pekola, J. P. Active quasiparticle suppression in a non-equilibrium superconductor. *Nano Lett.* **20**, 5065–5071 (2020).
130. Henriques, F. et al. Phonon traps reduce the quasiparticle density in superconducting circuits. *Appl. Phys. Lett.* **115**, 212601 (2019).
131. Rostem, K., de Visser, P. J. & Wollack, E. J. Enhanced quasiparticle lifetime in a superconductor by selective blocking of recombination phonons with a phononic crystal. *Phys. Rev. B* **98**, 014522 (2018).
132. Paladino, E., Galperin, Y., Falci, G. & Altshuler, B. 1/f noise: implications for solid-state quantum information. *Rev. Mod. Phys.* **86**, 361–418 (2014).
133. Shnirman, A., Schön, G., Martin, I. & Makhlin, Y. in *Electron Correlation in New Materials and Nanosystems* Vol. 241 [eds Scharnberg, K. & Kruchinin, S.] 343–356 (Springer, 2007).
134. Christensen, B. G. et al. Anomalous charge noise in superconducting qubits. *Phys. Rev. B* **100**, 140503 (2019).
135. Kumar, P. et al. Origin and reduction of 1/f magnetic flux noise in superconducting devices. *Phys. Rev. Appl.* **6**, 041001 (2016).
136. Anton, S. M. et al. Pure dephasing in flux qubits due to flux noise with spectral density scaling as $1/f^{\alpha}$. *Phys. Rev. B* **85**, 224505 (2012).
137. Van Harlingen, D. J., Plourde, B. L. T., Robertson, T. L., Reichardt, P. A. & Clarke, J. in *Decoherence in Flux Qubits due to 1/f Noise in Josephson Junctions* (eds Leggett, A. J., Ruggiero, B. & Silvestrini P.) 171–184 (Springer, 2004).
138. Constantin, M. & Yu, C. C. Microscopic model of critical current noise in Josephson junctions. *Phys. Rev. Lett.* **99**, 207001 (2007).
139. Schreier, J. A. et al. Suppressing charge noise decoherence in superconducting charge qubits. *Phys. Rev. B* **77**, 180502(R) (2008).
140. Murch, K. W., Weber, S. J., Levenson-Falk, E. M., Vijay, R. & Siddiqi, I. 1/f noise of Josephson-junction-embedded microwave resonators at single photon energies and millikelvin temperatures. *Appl. Phys. Lett.* **100**, 142601 (2012).
141. Dutta, P. & Horn, P. M. Low-frequency fluctuations in solids: 1/f noise. *Rev. Mod. Phys.* **53**, 497–516 (1981).
142. Atalaya, J., Clarke, J., Schön, G. & Shnirman, A. Flux 1/f noise in two-dimensional Heisenberg spin glasses: effects of weak anisotropic interactions. *Phys. Rev. B* **90**, 014206 (2014).
143. Choi, S., Lee, D.-H., Louie, S. G. & Clarke, J. Localization of metal-induced gap states at the metal-insulator interface: origin of flux noise in SQUIDs and superconducting qubits. *Phys. Rev. Lett.* **103**, 197001 (2009).
144. Voss, R. F. & Clarke, J. ‘1/f noise’ in music and speech. *Nature* **258**, 317–318 (1975).
145. Vion, D. Manipulating the quantum state of an electrical circuit. *Science* **296**, 886–889 (2002).
146. Deng, X.-H., Hu, Y. & Tian, L. Protecting superconducting qubits with a universal quantum degeneracy point. *Supercond. Sci. Technol.* **26**, 114002 (2013).
147. Kitaev, A. Fault-tolerant quantum computation by anyons. *Ann. Phys.* **303**, 2–30 (2003).
148. Lahtinen, V. & Pachos, J. A short introduction to topological quantum computation. *SciPost Phys.* **3**, 021 (2017).
149. Brooks, P., Kitaev, A. & Preskill, J. Protected gates for superconducting qubits. *Phys. Rev. A* **87**, 052306 (2013).
150. Gynis, A. et al. Experimental realization of an intrinsically error-protected superconducting qubit. *PRX Quantum* **2**, 10339 (2019).
151. Dempster, J. M., Fu, B., Ferguson, D. G., Schuster, D. I. & Koch, J. Understanding degenerate ground states of a protected quantum circuit in the presence of disorder. *Phys. Rev. B* **90**, 094518 (2014).
152. Groszkowski, P. et al. Coherence properties of the $0-\pi$ qubit. *N. J. Phys.* **20**, 043053 (2018).
153. Kitaev, A. Protected qubit based on a superconducting current mirror. Preprint at [arXiv](https://arxiv.org/abs/cond-mat/0609441) [https://arxiv.org/abs/cond-mat/0609441] (2006).
154. Peruzzo, M., Trioni, A., Hassani, F., Zemlicka, M. & Fink, J. M. Surpassing the resistance quantum with a geometric superinductor. *Phys. Rev. Appl.* **14**, 044055 (2020).
155. Zhang, W. *Applications of Superconductors in Superconducting Quantum Circuits*. Thesis, Rutgers Univ. (2019).
156. Masluk, N. A., Pop, I. M., Kamal, A., Minev, Z. K. & Devoret, M. H. Microwave characterization of Josephson junction arrays: implementing a low loss superinductance. *Phys. Rev. Lett.* **109**, 137002 (2012).
157. Niepe, D., Burnett, J. & Bylander, J. High kinetic inductance NbN nanowire superconductors. *Phys. Rev. Appl.* **11**, 044014 (2019).
158. Kamenov, P. et al. Granular aluminum meandered superconductors for quantum circuits. *Phys. Rev. Appl.* **13**, 054051 (2020).
159. Wang, J. I.-J. & Oliver, W. D. An aluminium superinductor. *Nat. Mater.* **18**, 775–776 (2019).
160. Grünhaupt, L. et al. Granular aluminium as a superconducting material for high-impedance quantum circuits. *Nat. Mater.* **18**, 816–819 (2019).
161. Gladchenko, S. et al. Superconducting nanocircuits for topologically protected qubits. *Nat. Phys.* **5**, 48–53 (2009).
162. Douçot, B., Feigel'man, M. V. & Ioffe, L. B. Topological order in the insulating Josephson junction array. *Phys. Rev. Lett.* **90**, 107003 (2003).
163. Bell, M. T., Paramanandam, J., Ioffe, L. B. & Gershenson, M. E. Protected Josephson rhombus chains. *Phys. Rev. Lett.* **112**, 167001 (2014).
164. Smith, W. C., Kou, A., Xiao, X., Vool, U. & Devoret, M. H. Superconducting circuit protected by two-Cooper-pair tunneling. *npj Quantum Inf.* **6**, 8 (2020).
165. Kalashnikov, K. et al. Bifluxon: fluxon-parity-protected superconducting qubit. *PRX Quantum* **1**, 010307 (2020).
166. Weides, M. *Barriers in Josephson Junctions: An Overview* Vol. 1 (Oxford Univ. Press, 2017).
167. Fritz, S., Schneider, R., Radtke, L., Weides, M. & Gerthsen, D. TEM investigations of Al/AIO_x/Al Josephson junctions. in *European Microscopy Congress 2016: Proceedings* (Wiley, 2016).
168. Weides, M. P. et al. Coherence in a transmon qubit with epitaxial tunnel junctions. *Appl. Phys. Lett.* **99**, 262502 (2011).
169. Kline, J. S. et al. Sub-micrometer epitaxial Josephson junctions for quantum circuits. *Supercond. Sci. Technol.* **25**, 025005 (2011).
170. Nakamura, Y. et al. Superconducting qubits consisting of epitaxially grown NbN/AlN/NbN Josephson junctions. *Appl. Phys. Lett.* **99**, 212502 (2011).
171. Liu, Y. et al. Van der Waals heterostructures and devices. *Nat. Rev. Mater.* **1**, 16042 (2016).
172. Girit, C. et al. Tunable graphene dc superconducting quantum interference device. *Nano Lett.* **9**, 198–199 (2009).
173. Wang, J. I.-J. et al. Coherent control of a hybrid superconducting circuit made with graphene-based van der Waals heterostructures. *Nat. Nanotechnol.* **14**, 120–125 (2019).
174. Xiao, Y., Liu, J. & Fu, L. Moiré is more: access to new properties of two-dimensional layered materials. *Matter* **3**, 1142–1161 (2020).
175. Lee, K.-H. et al. Two-dimensional material tunnel barrier for Josephson junctions and superconducting qubits. *Nano Lett.* **19**, 8287–8293 (2019).
176. Chiu, K.-L. et al. Flux tunable superconducting quantum circuit based on Weyl semimetal MoTe₂. *Nano Lett.* **20**, 8469–8475 (2020).
177. Yabuki, N. et al. Supercurrent in van der Waals Josephson junction. *Nat. Commun.* **7**, 10616 (2016).
178. Vijay, R., Sau, J. D., Cohen, M. L. & Siddiqi, I. Optimizing anharmonicity in nanoscale weak link Josephson junction oscillators. *Phys. Rev. Lett.* **103**, 087003 (2009).
179. Astafiev, O. V. et al. Coherent quantum phase slip. *Nature* **484**, 355–358 (2012).
180. Mooij, J. E. & Harmans, C. J. P. M. Phase-slip flux qubits. *N. J. Phys.* **7**, 219–219 (2005).
181. Li, Z.-Z., Li, T.-F., Lam, C.-H. & You, J. Q. Collective quantum phase slips in multiple nanowire junctions. *Phys. Rev. A* **99**, 012309 (2019).
182. Kenawy, A., Magnus, W., Milošević, M. V. & Sorée, B. Electronically tunable quantum phase slips in voltage-biased superconducting rings as a base for phase-slip flux qubits. *Supercond. Sci. Technol.* **33**, 125002 (2020).
183. Winkel, P. et al. Implementation of a transmon qubit using superconducting granular aluminum. *Phys. Rev. X* **10**, 031032 (2020).

Acknowledgements

This work was supported by the Office of Advanced Scientific Computing Research, Testbed Program, Office of Science of the US Department of Energy under contract no. DE-AC02-05CH11231. G. Catelani, J. Clarke, M. Devoret, L. Faoro, L. Glazman, L. Ioffe, A. Jordan, C. Müller, W. Oliver and J. Preskill provided critical comments on the manuscript. L. Nguyen provided the numerical data used in Fig. 2. J. M. Kreikebaum provided the chip photograph used in Fig. 3.

Competing interests

The author declares no competing interests.

Peer review information

Nature Reviews Materials thanks Hanhee Paik, Jonas Bylander and the other, anonymous, reviewer(s) for their contribution to the peer review of this work.

Publisher's note

Springer Nature remains neutral with regard to jurisdictional claims in published maps and institutional affiliations.

© Springer Nature Limited 2021